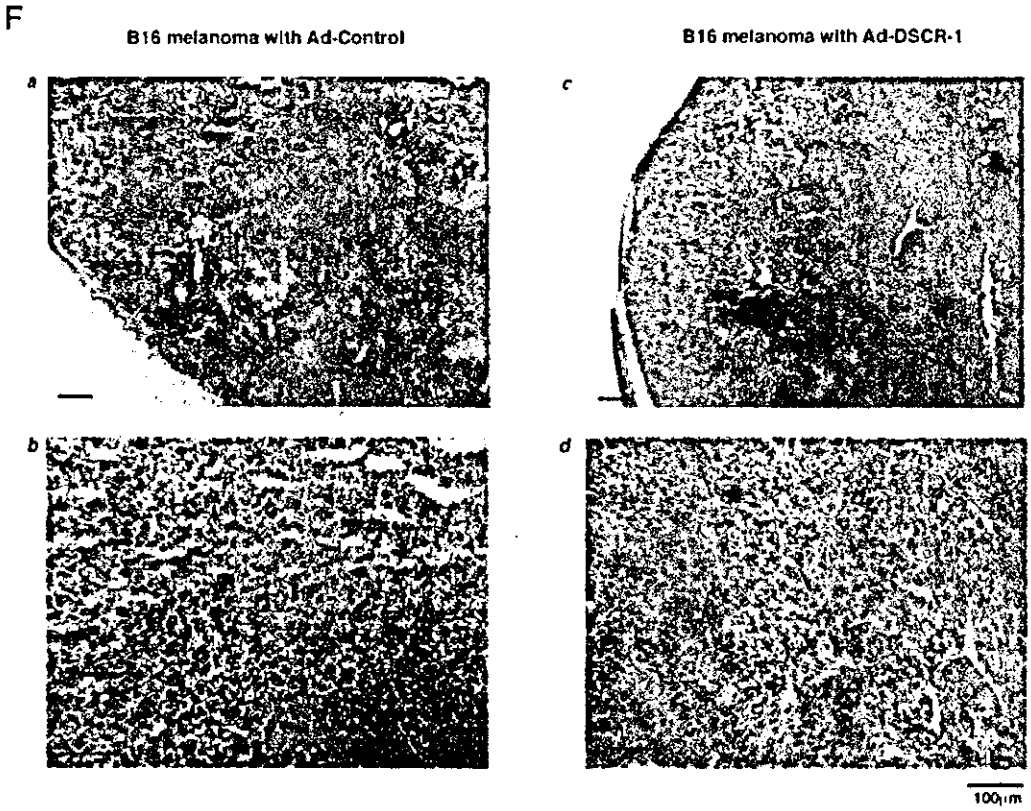

FIG. 7—*continued*

inhibited by the addition of 100-fold molar excess of unlabeled GATA mutant self-competitor but not a NF-AT mutant competitor. The DNA-protein complex was strongly supershifted by anti-NF-ATc antibody and only weakly supershifted by NF-ATp antibody (Fig. 5*F*, *lanes 3–6*). Similar results were obtained with nuclear extracts derived from thrombin-treated HUVEC (data not shown). The faster migrating DNA-protein complex includes NF-ATc, as it was specifically supershifted by anti-NF-ATc antibody (Fig. 5, *C*, *D*, and *F*, open arrows). Together with the transfection assays, the mobility shift results suggest that VEGF and thrombin induce DSCR-1 expression through the coordinate binding of NF-ATc and GATA-2/3 to closely positioned NF-AT and GATA motifs in the intragenic promoter.

DSCR-1 Inhibits Nuclear Localization of NF-ATc and Tube Formation in Primary Human Endothelial Cells—We next wished to determine the functional relevance of VEGF- and thrombin-mediated DSCR-1 induction. To that end, we infected HUVEC with IRES-containing adenoviruses expressing both DSCR-1 and EGFP (Ad-DSCR-1) or EGFP alone (Ad-Control). Adenovirus-mediated overexpression of DSCR-1, but not control EGFP, inhibited VEGF- and thrombin-mediated nuclear localization of NF-ATc at 1 h, 94.2 and 92.8%, respectively. (Fig. 6, *A* and *B*). In collagen gel assays of HUVEC, VEGF induced the formation of capillary or tube-like structures (compare Fig. 6*C*, *a* and *b*). Compared with Ad-Control, Ad-DSCR-1 infection resulted in marked reduction of tube formation (29.2% of basal level) under the same infection rate and EGFP expression levels (Fig. 6*C*, *panels b–h*, and *D*). Together with the transient transfection and EMSA results, the above findings suggest that VEGF and thrombin each induce the nuclear localization of NF-ATc, cooperative binding of NF-ATc and GATA-2/3 to the DSCR-1 promoter, secondary induction of DSCR-1 mRNA expression, and subsequent attenuation of NF-AT signaling and blood vessel growth.

DSCR-1 Attenuates Cell Proliferation of Primary Human Endothelial Cells—Angiogenesis involves a complex interplay of myriad cellular functions, including endothelial cell migration and proliferation. To evaluate the effect of DSCR-1 on cell proliferation, we performed FACS analysis with subconfluent HUVEC infected with either Ad-Control, Ad-DSCR-1, or Ad-DSCR-1 plus Ad-CA-NFAT. FACS analysis of Ad-Control-infected HUVEC (at 90% confluence) revealed 67.2, 17.7, and 15.1% in G_0/G_1, S, and G_2/M phases, respectively. Ad-mediated overexpression of DSCR-1 increased the percentage of cells in G_0/G_1 phase and decreased the fraction in S phase, an effect that was reversed by co-infection with Ad-CA-NFAT (Fig. 6*E*). Similar findings were obtained with HUVEC at 50% confluence (data not shown). Compared with Ad-Control, Ad-DSCR-1 did not result in increased apoptosis (Fig. 6*F*), arguing against a toxic effect of DSCR-1 overexpression. Taken together, these findings suggest that the constitutive DSCR-1 expression in endothelial cells induces G_0/G_1 arrest.

DSCR-1 Blocks Matrix Neo-vascularization and Tumor Progression in Mice—Having established an inhibitory role for DSCR-1 on cell cycle arrest and angiogenesis *in vitro*, we wished to evaluate the functional relevance of these findings *in vivo*. To that end, we investigated the effects of DSCR-1 overexpression on new blood vessel formation in a matrigel plug assay. In these experiments, matrigel containing either Ad-Control, Ad-DSCR-1, or Ad-DSCR-1 plus Ad-CA-NFAT was implanted as subcutaneous plugs into C57BL/6 mice. Fourteen days after implantation, cross-sections from control matrigel plugs demonstrated significant blood vessel formation (Fig. 7*A*, *left*). In contrast, overexpression of DSCR-1 in the matrigel markedly reduced plug vascularity (Fig. 7*A*, *middle*). Importantly, the inhibitory effect of DSCR-1 was rescued by co-infection with adenovirus expressing constitutive active NF-AT (Fig. 7*A*, *right*). To quantify the extent of neo-angiogenesis, we

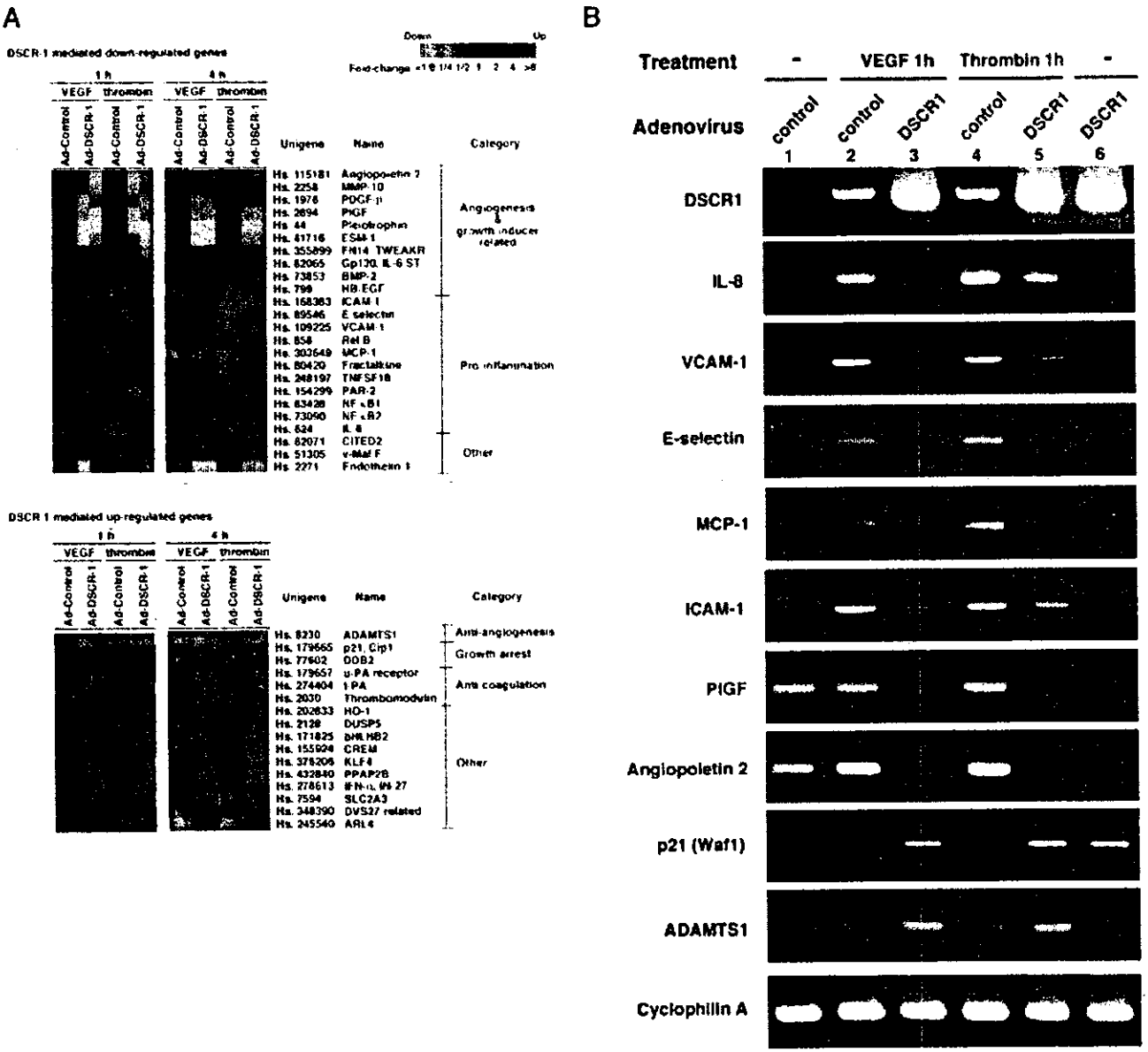

FIG. 8. **DSCR-1 attenuates VEGF- and thrombin-mediated induction of pro-angiogenesis and pro-inflammatory genes in primary endothelial cells.** *A*, DNA microarray studies demonstrating the effect of DSCR-1 overexpression on VEGF and thrombin-responsive genes in HUVEC. *B*, RT-PCR was performed with either Ad-Control (*lanes 1*, *2*, and *4*)- or Ad-DSCR-1 (*lanes 3*, *5*, and *6*)-infected HUVEC treated in the absence (−) (*lanes 1* and *6*) or presence of VEGF (*lanes 2* and *3*) or thrombin (*lanes 4* and *5*). Cyclophilin A indicates the internal control. The results are representative of at least two separate experiments.

measured hemoglobin content in the matrigel plugs. Matrigel that contained no virus or Ad-Control demonstrated comparable levels of angiogenesis. However, Ad-DSCR-1 resulted in a significant (67%) reduction of the hemoglobin content. This effect was reversed by co-expression of constitutively active NF-AT (Fig. 7*B*).

To evaluate whether DSCR-1 has anti-tumor activity, mice were injected subcutaneously with B16-melanoma cells. When tumor size reached 50 mm^3 in volume, the xenografts were injected with Ad-DSCR-1 or Ad-Control. Tumor mass was measured on each subsequent day (Fig. 7*C*). Compared with control, Ad-DSCR-1 treatment resulted in statistically significant reduction in blood vessel density and tumor size (Fig. 7, *D–F*). There was no difference in body weight between the groups (data not shown). Collectively, these findings suggest that DSCR-1, a negative feedback regulator of NF-AT signaling, acts as an inhibitor of angiogenesis.

DSCR-1 Overexpression in Primary Endothelial Cells Results in Down-regulation of Multiple Pro-angiogenic and Pro-inflammatory Genes—Finally, to gain insight into the broader role for DSCR-1 in auto-inhibition of VEGF and thrombin signaling, HUVEC were infected with Ad-Control or Ad-DSCR-1, treated in the absence or presence of VEGF or thrombin, and then processed for DNA microarray analyses. From the duplicate arrays, a total of 24 genes (from a total of 8974 genes) were induced by VEGF or thrombin and strongly reduced in the presence of DSCR-1 (Fig. 8*A*). Notably, 10 genes in this group are associated with cell proliferation and angiogenesis and 11 with inflammation. Interestingly, when the filter was changed to the DSCR-1-mediated up-regulated genes, a total of 16 genes emerged, including the cell cycle inhibitor, p21, anti-angiogenesis factor, ADAMTS1 (28), and anti-coagulation factors t-PA, u-PAR, and thrombomodulin (Fig. 8*A* and supplemental Table II). These results, many of which have been validated in RT-

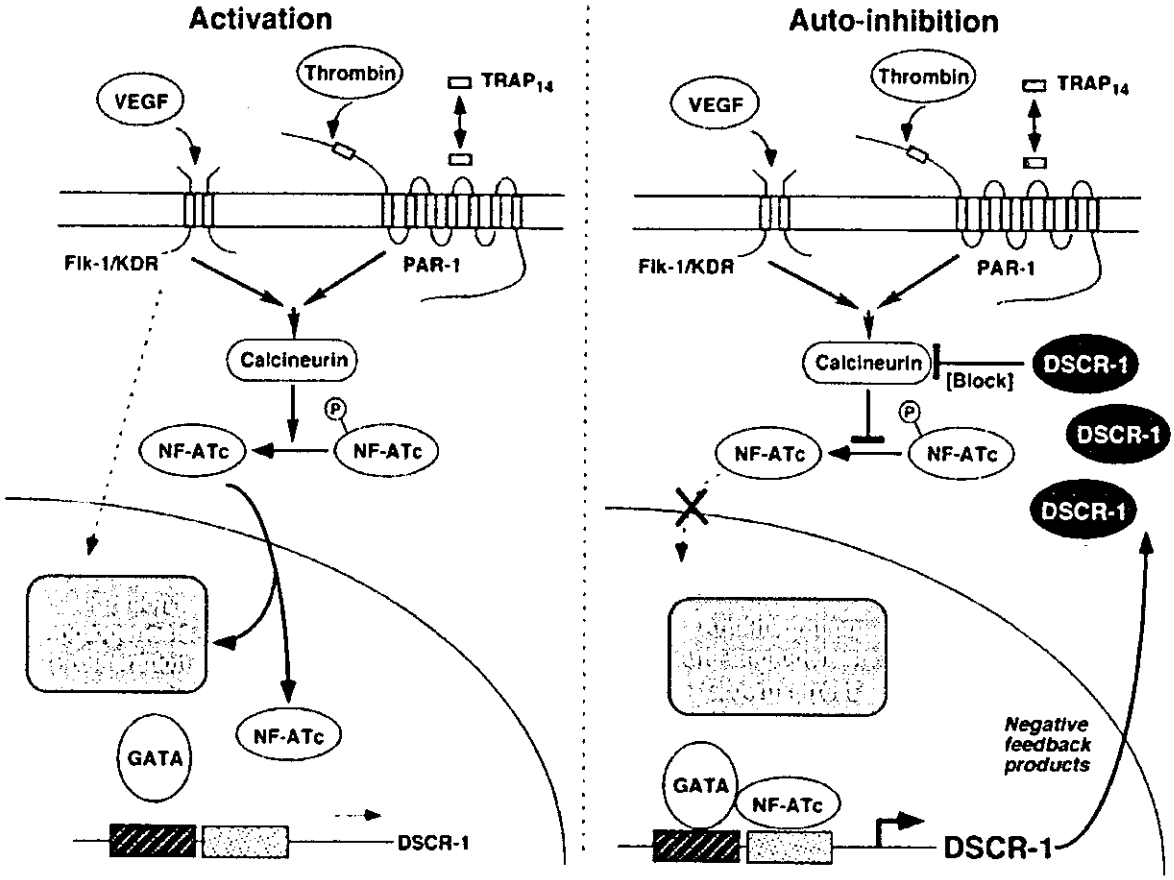

FIG. 9. **Model.** Schematic shows the VEGF or thrombin-calcineurin-NF-ATc signaling and the DSCR-1-mediated auto-inhibition system in endothelium.

PCR (Fig. 8*B*), suggest that DSCR-1 works as a key negative feedback regulator responding not only with VEGF- and thrombin-mediated angiogenesis and cell proliferation but also with inflammation and hemostatic balance.

DISCUSSION

The activation of endothelial cells by extracellular stimuli is a key mechanism underlying the development of many vascular diseases. In the present study, we have employed DNA microarrays to analyze the global gene expression profile of activated primary human endothelial cells and show that VEGF and thrombin, but not TNF-α, resulted in the rapid and pronounced induction of DSCR-1. Activated DSCR-1, in turn, profoundly attenuated calcineurin-dependent NF-AT signaling (see below). Thus, we hypothesize that DSCR-1 functions as a circuit breaker, ensuring balanced regulation of endothelial cell proliferation, migration, and angiogenesis (Fig. 9).

The VEGF and thrombin signals are transduced through calcineurin-dependent nuclear translocation of NF-AT. The NF-AT family of transcription factors includes four structurally related members, NF-ATp, NF-ATc, NF-AT3, and NF-AT4. NF-ATp and NF-ATc have been detected in endothelial cells (29–31). Previous studies in non-endothelial cells have shown that NF-AT cooperates with other transcription factors, including AP1 (32), GATA (33, 34), cMAF (35), or MEF2 (36), to enhance target gene expression. Among the functional sequelae of calcineurin-NF-AT signaling is immune response, cardiac and skeletal and vascular smooth muscle proliferation and/or hypertrophy (37), cardiac valve development (30, 38), differentiation of adipocytes and skeletal muscle (39, 40), synaptic plasticity, and cellular apoptosis. Here, we show that VEGF and thrombin induce the nuclear translocation of NF-ATc in HUVEC and that NF-ATc cooperates synergistically with GATA-2/3 to transactivate the DSCR-1 promoter. These data are consistent with our previous studies demonstrating an important role for the GATA family of transcription factors as signal transducers in the endothelium (20).

While previous investigations have established the importance of PI3K and MAPK signaling pathways in mediating endothelial cell survival, proliferation, and angiogenesis, comparatively little is known about the functional role for calcium-calcineurin signaling in these biological processes. Activated GSK-3β has been shown to promote the cytosol translocation of NF-AT (41, 42) and to negatively regulate endothelial cell proliferation and angiogenesis (43). Together with our results, these data support the notion that both calcineurin and PI3K-AKT-dependent inactivation of GSK-3β contribute to nuclear retention of NF-AT and secondary endothelial cell migration, growth, and angiogenesis.

Our data suggest that DSCR functions as an endogenous anti-angiogenic factor. In addition to its effect on nuclear localization of NF-ATc and tube formation in primary endothelial cells, DSCR-1 inhibited endothelial cell migration and promoted G_0/G_1 cell cycle arrest. Most importantly, DSCR-1 blocked matrix neo-vascularization and tumor progression in mice. Moreover, in repeated microarray studies, overexpression of DSCR-1 resulted in down-regulation of pro-angiogenic factors such as PlGF, angiopoietin-2, BMP-2, and PDGF-B and up-regulation of the growth-arrest factors p21 and anti-angiogenic factor ADAMTS1 (28). It will be interesting to determine whether DSCR-1 expression is modulated in tumor endothe-

lium and whether such changes are correlated with tumor growth and/or metastases. From a therapeutic perspective, our results point to a potential benefit of overexpressing and/or inducing the activity of DSCR-1 in tumor endothelium.

In addition to its inhibitory effect on endothelial cell proliferation and angiogenesis, DSCR-1 was also shown to down-regulate the expression of a number of activation markers in endothelial cells, including ICAM-1, VCAM-1, tissue factor, interleukin-8, and E-selectin. These results are consistent with previous studies demonstrating a link between calcineurin-NF-AT and a pro-inflammatory response. For example, in endothelial cells, CsA-sensitive induction of NF-AT-mediated has been implicated in the expression of granulocyte macrophage colony-stimulating factor and E-selectin (29). Histamine induces interleukin-8 in HUVEC through a CsA-sensitive, NF-AT-dependent mechanism (44). A previous study in HUVEC demonstrated that VEGF induces tissue factor expression via a calcineurin-NF-AT/AP1-dependent mechanism (31). Taken together, these data suggest that DSCR-1 may exert an auto-inhibitory break on Ca^{2+}-calcineurin-NF-AT-mediated endothelial cell activation.

Such a mechanism is reminiscent of the NF-κB-I-κBα auto-inhibitory loop. Cellular activation results in phosphorylation-dependent degradation and subsequent ubiquitination of I-κBα. As a result, RelA translocates to the nucleus and partners with other members of the NF-κB family to transactivate a multitude of target genes, including pro-inflammatory mediators. In addition, the NF-κB family induces the early expression of its inhibitor, I-κBα (3, 4), which serves to dampen further RelA activity. Consistent with these results, we have shown that VEGF, thrombin, and TNF-α each results in the rapid induction of I-κBα in HUVEC, an effect that is blocked by pretreatment with proteasome inhibitors and enhanced by cyclohexamide (data not shown). The NF-AT-DSCR and NF-κB-I-κBα negative feedback loops may function to "fine tune" the desired downstream effect of the transcription factor and signal transducer.

During the preparation of this manuscript, Hesser *et al.* (45) reported that VEGF, but not basic fibroblast growth factor, induces DSCR-1 mRNA and protein in HUVEC. They showed that this occurs through Flk-1/KDR and involves a Cn-dependent mechanism. Finally, consistent with our results, they demonstrated that DSCR-1 suppressed the expression of inflammatory marker genes in activated endothelial cells (45). However, there are several important differences between the two studies. First, Hesser *et al.* (45) reported that VEGF and TNF-α induce comparable levels of DSCR-1 mRNA at 6 h. In our study, we show that VEGF has a much greater effect compared with TNF-α on DSCR-1 mRNA at 1 h. Second, we have demonstrated that thrombin induces DSCR-1 expression, suggesting that the auto-inhibitory loop is not specific to VEGF signaling. Third, and most importantly, we have extended the studies to show that DSCR-1 also inhibits VEGF-mediated effects on endothelial cell migration, cell cycle progression, and tube formation in primary human endothelial cells, as well as neo-vascularization and tumor progression in mice.

An important goal in vascular biology is to understand the molecular mechanisms by which the microenvironment regulates vascular function in space and time. In this study, we have analyzed the effect of VEGF and thrombin signals on endothelial cell gene expression and demonstrated a key role for DSCR-1 as a negative feedback regulator common to both mediators. Based on this knowledge, we believe that DSCR-1 may lend itself to therapeutic manipulation in vasculopathic disease states, including tumor angiogenesis.

Acknowledgments—We are grateful to Dr. Stuart H. Orkin for providing the GATA-2 expression vector (pMT_2-GATA2) and Drs. Syoichiro Miyatake and Naoko Arai for providing the CA-NF-AT expression vector (pSRα-CA-NFAT).

REFERENCES

1. Baeuerle, P. A., and Baltimore, D. (1988) *Science* **242,** 540–546
2. Baeuerle, P. A., and Baltimore, D. (1989) *Genes Dev.* **3,** 1689–1698
3. Scott, M. L., Fujita, T., Liou, H. C., Nolan, G. P., and Baltimore, D. (1993) *Genes Dev.* **7,** 1266–1276
4. Hoffmann, A., Levchenko, A., Scott, M. L., and Baltimore, D. (2002) *Science* **298,** 1241–1245
5. Isner, J. M., and Losordo, D. W. (1999) *Nat. Med.* **5,** 491–492
6. Ferrara, N. (2001) *Am. J. Physiol.* **280,** C1358–C1366
7. Quinn, T. P., Peters, K. G., De Vries, C., Ferrara, N., and Williams, L. T. (1993) *Proc. Natl. Acad. Sci. U. S. A.* **90,** 7533–7537
8. de Vries, C., Escobedo, J. A., Ueno, H., Houck, K., Ferrara, N., and Williams, L. T. (1992) *Science* **255,** 989–991
9. Soker, S., Takashima, S., Miao, H. Q., Neufeld, G., and Klagsbrun, M. (1998) *Cell* **92,** 735–745
10. Xia, P., Aiello, L. P., Ishii, H., Jiang, Z. Y., Park, D. J., Robinson, G. S., Takagi, H., Newsome, W. P., Jirousek, M. R., and King, G. L. (1996) *J. Clin. Invest.* **98,** 2018–2026
11. Fujio, Y., and Walsh, K. (1999) *J. Biol. Chem.* **274,** 16349–16354
12. Kroll, J., and Waltenberger, J. (1997) *J. Biol. Chem.* **272,** 32521–32527
13. Rousseau, S., Houle, F., Landry, J., and Huot, J. (1997) *Oncogene* **15,** 2169–2177
14. Gille, H., Kowalski, J., Li, B., LeCouter, J., Moffat, B., Zioncheck, T. F., Pelletier, N., and Ferrara, N. (2001) *J. Biol. Chem.* **276,** 3222–3230
15. Minami, T., Sugiyama, A., Wu, S. Q., Abid, R., Kodama, T., and Aird, W. C. (2004) *Arterioscler. Thromb. Vasc. Biol.* **24,** 41–53
16. Coughlin, S. R. (2000) *Nature* **407,** 258–264
17. O'Brien, P. J., Prevost, N., Molino, M., Hollinger, M. K., Woolkalis, M. J., Woulfe, D. S., and Brass, L. F. (2000) *J. Biol. Chem.* **275,** 13502–13509
18. Minami, T., Abid, M. R., Zhang, J., King, G., Kodama, T., and Aird, W. C. (2003) *J. Biol. Chem.* **278,** 6976–6984
19. Klee, C. B., Ren, H., and Wang, X. (1998) *J. Biol. Chem.* **273,** 13367–13370
20. Minami, T., and Aird, W. C. (2001) *J. Biol. Chem.* **276,** 47632–47641
21. Dignam, J. D., Martin, P. L., Shastry, B. S., and Roeder, R. G. (1983) *Methods Enzymol.* **101,** 582–598
22. Minami, T., Murakami, T., Horiuchi, K., Miura, M., Noguchi, T., Miyazaki, J., Hamakubo, T., Aird, W. C., and Kodama, T. (2004) *J. Biol. Chem.* **279,** 20626–20635
23. Fuentes, J. J., Pritchard, M. A., and Estivill, X. (1997) *Genomics* **44,** 358–361
24. Yang, J., Rothermel, B., Vega, R. B., Frey, N., McKinsey, T. A., Olson, E. N., Bassel-Duby, R., and Williams, R. S. (2000) *Circ. Res.* **87,** E61–E68
25. Wang, Y., De Keulenaer, G. W., Weinberg, E. O., Muangman, S., Gualberto, A., Landschulz, K. T., Turi, T. G., Thompson, J. F., and Lee, R. T. (2002) *Am. J. Physiol.* **283,** H533–H539
26. Rothermel, B., Vega, R. B., Yang, J., Wu, H., Bassel-Duby, R., and Williams, R. S. (2000) *J. Biol. Chem.* **275,** 8719–8725
27. Molkentin, J. D., Lu, J. R., Antos, C. L., Markham, B., Richardson, J., Robbins, J., Grant, S. R., and Olson, E. N. (1998) *Cell* **93,** 215–228
28. Luque, A., Carpizo, D. R., and Iruela-Arispe, M. L. (2003) *J. Biol. Chem.* **278,** 23656–23665
29. Cockerill, G. W., Bert, A. G., Ryan, G. R., Gamble, J. R., Vadas, M. A., and Cockerill, P. N. (1995) *Blood* **86,** 2689–2698
30. de la Pompa, J. L., Timmerman, L. A., Takimoto, H., Yoshida, H., Elia, A. J., Samper, E., Potter, J., Wakeham, A., Marengere, L., Langille, B. L., Crabtree, G. R., and Mak, T. W. (1998) *Nature* **392,** 182–186
31. Armesilla, A. L., Lorenzo, E., Gomez del Arco, P., Martinez-Martinez, S., Alfranca, A., and Redondo, J. M. (1999) *Mol. Cell. Biol.* **19,** 2032–2043
32. Rao, A., Luo, C., and Hogan, P. G. (1997) *Annu. Rev. Immunol.* **15,** 707–747
33. Musaro, A., McCullagh, K. J., Naya, F. J., Olson, E. N., and Rosenthal, N. (1999) *Nature* **400,** 581–585
34. Wada, H., Hasegawa, K., Morimoto, T., Kakita, T., Yanazume, T., Abe, M., and Sasayama, S. (2002) *J. Cell Biol.* **156,** 983–991
35. Ho, I. C., Hodge, M. R., Rooney, J. W., and Glimcher, L. H. (1996) *Cell* **85,** 973–983
36. Mao, Z., Bonni, A., Xia, F., Nadal-Vicens, M., and Greenberg, M. E. (1999) *Science* **286,** 785–790
37. Yellaturu, C. R., Ghosh, S. K., Rao, R. K., Jennings, L. K., Hassid, A., and Rao, G. N. (2002) *Biochem. J.* **368,** 183–190
38. Ranger, A. M., Grusby, M. J., Hodge, M. R., Gravallese, E. M., de la Brousse, F. C., Hoey, T., Mickanin, C., Baldwin, H. S., and Glimcher, L. H. (1998) *Nature* **392,** 186–190
39. Ho, I. C., Kim, J. H., Rooney, J. W., Spiegelman, B. M., and Glimcher, L. H. (1998) *Proc. Natl. Acad. Sci. U. S. A.* **95,** 15537–15541
40. Chin, E. R., Olson, E. N., Richardson, J. A., Yang, Q., Humphries, C., Shelton, J. M., Wu, H., Zhu, W., Bassel-Duby, R., and Williams, R. S. (1998) *Genes Dev.* **12,** 2499–2509
41. Beals, C. R., Sheridan, C. M., Turck, C. W., Gardner, P., and Crabtree, G. R. (1997) *Science* **275,** 1930–1934
42. Neal, J. W., and Clipstone, N. A. (2001) *J. Biol. Chem.* **276,** 3666–3673
43. Kim, H. S., Skurk, C., Thomas, S. R., Bialik, A., Suhara, T., Kureishi, Y., Birnbaum, M., Keaney, J. F., Jr., and Walsh, K. (2002) *J. Biol. Chem.* **277,** 41888–41896
44. Boss, V., Wang, X., Koppelman, L. F., Xu, K., and Murphy, T. J. (1998) *Mol. Pharmacol.* **54,** 264–272
45. Hesser, B. A., Liang, X. H., Camenisch, G., Yang, S., Lewin, D. A., Scheller, R., Ferrara, N., and Gerber, H. P. (2004) *Blood* **104,** 149–158

THE JOURNAL OF BIOLOGICAL CHEMISTRY
Vol. 279, No. 39, Issue of September 24, pp. 41114–41123, 2004
Printed in U.S.A.

Skeletal Muscle FOXO1 (FKHR) Transgenic Mice Have Less Skeletal Muscle Mass, Down-regulated Type I (Slow Twitch/Red Muscle) Fiber Genes, and Impaired Glycemic Control*[S]

Received for publication, January 21, 2004, and in revised form, July 9, 2004
Published, JBC Papers in Press, July 21, 2004, DOI 10.1074/jbc.M400674200

Yasutomi Kamei‡§¶, Shinji Miura§, Miki Suzuki§, Yuko Kai§, Junko Mizukami‖, Tomoyasu Taniguchi‖, Keiji Mochida, Tomoko Hata‡‡, Junichiro Matsuda‡‡, Hiroyuki Aburatani§§, Ichizo Nishino¶¶, and Osamu Ezaki§**

*From the ‡PRESTO, Japan Science and Technology Agency, §Division of Clinical Nutrition, National Institute of Health and Nutrition, 1-23-1 Toyama, Shinjuku-ku, Tokyo 162-8636, ‖Lead Generation Research Laboratory, Tanabe Seiyaku Co., Ltd., 3-16-89 Kashima, Yodogawa-ku, Osaka 532-8505, **Bioresource Center, Institute of Physical and Chemical Research, 3-1-1 Koyadai, Tsukuba-shi, Ibaraki 305-0074, the ‡‡Department of Veterinary Science, National Institute of Infectious Diseases, 1-23-1 Toyama, Shinjuku-ku, Tokyo 162-8640, §§Research Center for Advanced Science and Technology, University of Tokyo, 4-6-1 Komaba, Meguro-ku, Tokyo 153-8904, and the ¶¶Department of Neuromuscular Research, National Institute of Neuroscience, National Center of Neurology and Psychiatry, 4-1-1 Ogawahigashi-cho, Kodaira, Tokyo 187-8502, Japan*

FOXO1, a member of the FOXO forkhead type transcription factors, is markedly up-regulated in skeletal muscle in energy-deprived states such as fasting and severe diabetes, but its functions in skeletal muscle have remained poorly understood. In this study, we created transgenic mice specifically overexpressing FOXO1 in skeletal muscle. These mice weighed less than the wild-type control mice, had a reduced skeletal muscle mass, and the muscle was paler in color. Microarray analysis revealed that the expression of many genes related to the structural proteins of type I muscles (slow twitch, red muscle) was decreased. Histological analyses showed a marked decrease in size of both type I and type II fibers and a significant decrease in the number of type I fibers in the skeletal muscle of FOXO1 mice. Enhanced gene expression of a lysosomal proteinase, cathepsin L, which is known to be up-regulated during skeletal muscle atrophy, suggested increased protein degradation in the skeletal muscle of FOXO1 mice. Running wheel activity (spontaneous locomotive activity) was significantly reduced in FOXO1 mice compared with control mice. Moreover, the FOXO1 mice showed impaired glycemic control after oral glucose and intraperitoneal insulin administration. These results suggest that FOXO1 negatively regulates skeletal muscle mass and type I fiber gene expression and leads to impaired skeletal muscle function. Activation of FOXO1 may be involved in the pathogenesis of sarcopenia, the age-related decline in muscle mass in humans, which leads to obesity and diabetes.

Skeletal muscle is the largest organ in the human body, comprising about 40% of the body weight. The mass and composition of skeletal muscle are critical for its functions, such as exercise, energy expenditure, and glucose metabolism (1, 2). Elderly humans are known to undergo a progressive loss of muscle fibers associated with diabetes, obesity, and decreased physical activity (sarcopenia) (3). In human skeletal muscle, there are two major classifications of fiber type: type I (slow-twitch oxidative, so-called red muscle) and type II (fast-twitch glycolytic, so-called white muscle) fibers (2). Mass, fiber size, and fiber composition in adult skeletal muscle are regulated in response to changes in physical activity, environment, or pathological conditions. For example, space flight experiments using rats showed a reduction in total skeletal muscle mass of up to 37% as well as a significant loss of contractile proteins in type I but not type II fibers by 1–2 weeks of microgravity (4). Furthermore, the ratio of type I to type II fibers is associated with obesity and diabetes; the number of type I fibers is reduced in obese subjects and diabetic subjects compared with that in controls (5–7).

Skeletal muscle mass is positively regulated by hormones such as insulin-like growth factors (IGFs)[1] and growth hormone (8). Induction of hypertrophy in adult skeletal muscle by increased load is accompanied by the increased expression of IGF-1 (9). Systemic administration of IGF-1 results in increased skeletal muscle protein and reduced protein degradation (10). In addition, overexpression of IGF-1 blocks the age-related loss of skeletal muscle (11). Supplementation of IGF-1 to muscle cells *in vitro* promotes myotube hypertrophy, suggesting that hypertrophy can be mediated by autocrine- or paracrine-produced IGF-1 (12). Thus, delivery of the *IGF-1* gene specifically into skeletal muscle has been proposed as a genetic therapy for skeletal muscle disorders. A better understanding of the role of IGF-1 in skeletal muscle is therefore of great importance.

Specialized/differentiated myofiber phenotypes, including type I and type II fibers, are plastic and are physiologically

* This work was supported in part by research grants from the Japanese Ministry of Health, Labor, and Welfare (Tokyo) and by a grant from the Promotion of Fundamental Studies in Health Sciences of the Organization for Pharmaceutical Safety and Research. The costs of publication of this article were defrayed in part by the payment of page charges. This article must therefore be hereby marked "*advertisement*" in accordance with 18 U.S.C. Section 1734 solely to indicate this fact.

[S] The on-line version of this article (available at http://www.jbc.org) contains Information 1 and 2.

¶ To whom correspondence should be addressed: Division of Clinical Nutrition, National Institute of Health and Nutrition, 1-23-1 Toyama, Shinjuku-ku, Tokyo 162-8636, Japan. Tel.: 81-3-3203-5725; Fax: 81-3-3207-3520; E-mail: ykamei@nih.go.jp.

[1] The abbreviations used are: IGF, insulin-like growth factor; CaMK, calmodulin-dependent kinase; PGC-1α, peroxisome proliferator activated receptor-γ coactivator-1α; STZ, streptozotocin; MLC, myosin light chain; mtCK, mitochondrial creatine kinase; IGFBP, IGF-binding protein; COX, cytochrome *c* oxidase; DEXA, dual energy X-ray absorptiometry; EDL, extensor digitorum longus.

controlled by variations in motor neuron activity. The influence of motor neuron activity on different types of skeletal muscle fibers is considered to be transduced via calcium signaling and downstream molecules such as calcineurin and the calmodulin-dependent kinase (CaMK) pathway (13). Signals generated by calcium/calcineurin/CaMK augment the transactivating function of Mef2 and/or NFAT and enhance type I fiber-specific gene expression (13–18). More recently, it has been shown that a nuclear receptor cofactor (19, 20), peroxisome proliferator activated receptor-γ coactivator-1α (PGC-1α) (21), drives the formation of type I fibers. Specifically, in transgenic mice expressing PGC-1α, type II fibers are red in color, and PGC-1α activates expression of type I fiber-specific genes (22). We also reproduced the PGC-1α-induced red appearance of skeletal muscle; both type I and type II fibers appear redder in transgenic mice overexpressing PGC-1α in skeletal muscle (23).

FOXO1 (FKHR), FOXO4 (AFX), and FOXO3a (FKHRL1) are a subfamily of the forkhead type transcription factors (24, 25). FOXO1 was originally cloned from a rhabdomyosarcoma because of its aberrant fusion with another transcription factor, PAX3, resulting from a chromosomal translocation (26). Recent studies have shown that the FOXO protein can also act as a cofactor of nuclear receptor activity (27–30). FOXO family members have been shown to regulate various cellular functions. FOXOs influence the transcription of genes involved in metabolism (31–34), the cell cycle (35, 36), and apoptosis (37, 38). In addition, FOXO1 can modulate cell differentiation; the constitutive active form of FOXO1 prevents the differentiation of preadipocytes (39) and stimulates myotube fusion of primary mouse myoblasts (40). Moreover, a FOXO1 knockout mouse has been reported; *Foxo1* haploinsufficiency restores insulin sensitivity and rescues the diabetic phenotype in insulin-resistant mice by reducing the hepatic expression of glucogenetic genes and by increasing the adipocytic expression of insulin-sensitizing genes (41). We have shown that FOXO1 expression is increased in skeletal muscle in energy-deprived states, such as in fasting mice, in mice with streptozotocin (STZ)-induced diabetes, and in mice after treadmill running (42). However, the physiological role of FOXO1 in skeletal muscle is still unclear. Although many studies have been performed using cultured cells, studies using animals with genetic modifications focused to the skeletal muscle remain to be conducted in order to understand the function of the FOXO family proteins *in vivo*. Meanwhile, it has been reported that FOXO1 and PGC-1α can physically interact and regulate gene expression in the liver (43). Given that PGC-1α is important for the differentiation of type I fibers, FOXO1 might be involved in this process. (Hereafter, we use "differentiation of muscle fiber" to mean "a switch from one fiber type to another fiber type.") On the other hand, a genetic study of *Caenorhabditis elegans* showed that DAF16, the worm counterpart of FOXO, functions as a suppressor of insulin receptor-like signaling (44). Thus, the FOXO family may act negatively in mammals as a downstream player in insulin or IGF signaling. As IGF-1 plays an important role in controlling skeletal muscle mass, FOXO1 might also be involved in this process.

To gain insight into the potential role of FOXO1 in skeletal muscle, including the control of skeletal muscle mass and the control of differentiation of muscle fiber type, we established transgenic mice specifically overexpressing FOXO1 in their skeletal muscle. Most interestingly, these mice showed reduced skeletal muscle mass, and the muscle was paler in color. Histochemical, physiological, and microarray analyses of these FOXO1 transgenic mice showed that FOXO1 is involved in the regulation of skeletal muscle mass and type I fiber gene expression. In addition, our results suggest that FOXO1 activation may play a role in the impairment of skeletal muscle function including glycemic control.

EXPERIMENTAL PROCEDURES

RNA Analysis—Northern blot analyses were performed as described previously (42). The cDNA probes for Gadd45α (GenBank™ accession number, U00937), troponin C (slow) (M29793), troponin T (slow) (AV213431), myosin light chain (MLC) (slow) (M91602), myoglobin (X04405), mitochondrial creatine kinase (mtCK, AV250974), F_0,F_1-ATPase (AF030559), MLC (fast) (U77943), troponin I (fast) (J04992), troponin T (fast) (L48989), cathepsin L (X06086), IGF-binding protein 5 (IGFBP5) (L12447), MuRF1 (AF294790), and atrogin 1 (AF441120) were obtained by reverse transcription-PCR. The PCR primers used are as follows: Gadd45α, forward, 5′-TCGCACTTGCAATATGACTT-3′, and reverse, 5′-CGGATGCCATCACCGTTCCG-3′; troponin C (slow), forward, 5′-AGCTGCCGGTAGAACAGTTGA-3′, and reverse, 5′-TCACCTGTGGCCTGCAGCAT-3′; troponin T (slow), forward, 5′-TTCTGTCCAACATGGGAGCT-3′, and reverse, 5′-TCGGAATTTCTGGGCGTGGC-3′; MLC (slow), forward, 5′-GAGTTCAAGGAAGCCTTCAC-3′, and reverse, 5′-CTGCGAACATCTGGTCGATC-3′; myoglobin, forward, 5′-CACCATGGGGCTCAGTGATG-3′, and reverse, 5′-CTCAGCCCTGGAAGCCTAGC-3′; mtCK, forward, 5′-AAAGGAAGTGGAACGATTAA-3′, and reverse, 5′-TTGATGTCTTGGCCTCTCTC-3′, F_0,F_1-ATPase, forward, 5′-ACTGACCCTGCCCCTGCAAC-3′, and reverse, 5′-CAAGGCTCTTGTGTGGCCTG-3′, MLC (fast), forward, 5′-AGGGATGGCATTATCGACAA-3′, and reverse, 5′-CAGATGTTCTTGTAGTCCAC-3′; troponin I, (fast), forward, 5′-AGGAAAGCCGCCGAGAATCT-3′, and reverse, 5′-TACTGGGGAAGTGGGCAGTT-3′; troponin T (fast), forward, 5′-CAGCAAAGAATTCGCGCTGA-3′, and reverse, 5′-GGCCTTCTTGCTGTGCTTCT-3′; cathepsin L, forward, 5′-CGGAGGAGTCTTACCCCTAT-3′, and reverse, 5′-CTACCCATCAATTCACGACA-3′; IGFBP5, forward, 5′-GCCTATGCCGTACCGGCTCA-3′, and reverse, 5′-CTTCACAGCCTCAGCCTTCA-3′; MuRF1, forward, 5′-ATGAACTTCACGGTGGGTTT-3′, and reverse, 5′-TCAGTGCAGGCCTGAGCCTT-3′; and atrogin 1, forward, 5′-ATGCCGTTCCTTGGGCAGGA-3′, and reverse, 5′-TCAGAACTTGAACAAATTGA-3′. FOXO1, FOXO3a, and FOXO4 cDNA probes were prepared as reported previously (42). COXII, COXIV, Mef2c, PGC-1α, and glucose transporter 4 cDNA probes were prepared as described previously (23). NFAT (IMAGE clone 4109469) and CaMK IIβ (IMAGE clone 5014712) cDNA probes were purchased from Invitrogen.

Generating Transgenic Mice—The human skeletal muscle α-actin promoter (45) was provided by Drs. E. D. Hardeman and K. Guven (Children's Medical Research Institute, Australia). The human FOXO1 cDNA was as described previously (42). The transgene (Fig. 1*A*) was excised from agarose gel and purified for injection (2 ng μl^{-1}). Fertilized eggs were recovered from C57BL/6 females crossed with C57BL/6 males and microinjected at Japan SLC Inc. (Hamamatsu, Japan). The mice were maintained at a constant temperature of 22 °C with fixed artificial light (12-h light and 12-h dark cycle). Care of the mice was conducted in accordance with the institutional guidelines.

Body Composition Analysis—Mice were anesthetized with pentobarbital sodium, Nembutal (0.08 mg/g body weight, Abbott), and scanned with a Lunar PIXI mus2 densitometer (Lunar Corp., Madison, WI), equipped for dual energy x-ray absorptiometry (DEXA) (46).

Immunoblotting—Protein extracts from skeletal muscle were prepared by centrifugation of the tissue homogenates as described previously (47). Protein extracts (30 μg) separated by SDS-PAGE were electrophoretically transferred to Immobilon P membranes (Millipore, Bedford, MA). Immunoblotting was performed by using goat anti-FOXO1 IgG (N-18, Santa Cruz Biotechnology, Inc. Santa Cruz, CA), goat anti-troponin I (slow) (C-19, Santa Cruz Biotechnology), goat anti-troponin I (fast) (C-19, Santa Cruz Biotechnology), goat anti-myoglobin (M-109, Santa Cruz Biotechnology), or rabbit anti-PGC-1α (C terminus, Calbiochem) as primary antibodies (1:1000) and anti-goat IgG or anti-rabbit IgG conjugated with horseradish peroxidase as secondary antibodies (1:1000). Bands were visualized with the enhanced chemiluminescence system (Amersham Biosciences).

Histological Analyses—Skeletal muscle (soleus) samples were frozen in liquid nitrogen-cooled isopentane, and transverse serial sections were stained with ATPase at pH 4.3 to detect type I fibers and at pH 10.5 to detect type II fibers (48). The ratio of type I fibers to type II fibers and the size (area) of skeletal muscle cells were determined by counting cell numbers in six randomly selected cross-section areas (each 900 μm^2) stained with ATPase at pH 4.3.

Blood Analysis—Blood samples were obtained from mice tail tips for hormone and metabolite determination under feeding conditions. Immunoreactive insulin was measured by an insulin assay kit (Morinaga,

Kanagawa, Japan), free fatty acid by NEFA C-test Wako (Wako Biochemicals, Osaka, Japan), lactate by the lactate reagent (Sigma), and glucose by the TIDEX glucose analyzer (Sankyo, Tokyo, Japan).

Running Wheel Activity—Mice were housed individually in cages (9 × 22 × 9 cm) equipped with a running wheel (20-cm in diameter, Shinano Co., Tokyo, Japan). Each wheel revolution was registered by a magnetic switch, which was connected to a counter. The number of revolutions was recorded daily for 6 days.

Oral Glucose and Insulin Tolerance Test—For the oral glucose tolerance test, D-glucose (1 mg/g of body weight, 10% (w/v) glucose solution) was administered with a stomach tube after an overnight fast. Blood samples were obtained by cutting the tail tip before and 30, 60, and 120 min after glucose administration. For the insulin tolerance test, human insulin (Humulin R; Lilly) was injected intraperitoneally (0.75 milliunits/g of body weight) into fed animals. Blood glucose concentrations were measured using a TIDEX glucose analyzer (Sankyo, Tokyo, Japan).

Microarray Analyses—RNA was isolated from skeletal muscle (quadriceps) of sex- and age-matched FOXO1 mice (A1 and A2 lines) and control mice (males at 4 months of age, RNA from three mice of each group were combined). Each of the combined samples was hybridized to the Affymetrix MGU74A microarray, which contains 12,489 genes including ESTs, and analyzed with the Affymetrix Gene Chip 3.1 software as described previously (49). Of the 12,489 genes including ESTs analyzed, 2500 (nontransgenic control mice), 2490 (line A1, transgenic), and 2510 (line A2, transgenic) genes were expressed at a substantial level (absolute call is present and average difference is above 150). Genes were classified on the basis of the biological function of the encoded protein, using a previously established classification scheme (50). The classification scheme was composed of seven major functional categories and several minor functional categories within the major categories.

Statistical Analyses—Statistical comparisons of data from the experimental groups were performed by the one-way analysis of variance, and groups were compared using the Fisher's protected least significant difference test (Statview 5.0, Abacus Concepts, Inc., Berkeley, CA). The glucose and insulin tolerance curves were compared by repeated measure analysis (Statview 5.0, Abacus Concepts). When significant, groups were compared by the Fisher's protected least significant difference test. Statistical significance was defined as $p < 0.05$.

RESULTS

Creation of FOXO1 Mice—The human skeletal muscle α-actin promoter (45) was used to drive the expression of the human *FOXO1* transgene in mice (Fig. 1*A*). During development, cardiac muscle α-actin is the predominant isoform of sarcomeric α-actin in mice, and the switch to skeletal muscle α-actin occurs postpartum (45). Thus, by using the skeletal muscle α-actin promoter, the possibility that embryonic expression of FOXO1 might interfere with development was minimized. We obtained two independent lines of transgenic mice (lines A1 and A2). Southern blot analysis of DNA obtained from mouse tails was performed as shown in Fig. 1*B*. The transgene copy number of each animal was estimated by densitometric scanning of the autoradiographs from the Southern blots.

Expression of the *FOXO1* transgene was evaluated by Northern blot analysis with RNA isolated from the tissues of FOXO1 mice and age-matched control mice at 8 weeks of age (Fig. 1*C*). The use of this promoter resulted in predominantly high expression levels of the *FOXO1* transgene in skeletal muscle (about 3.5 kb). The A2 line showed expression levels of the *FOXO1* transgene in skeletal muscle that were similar to or slightly higher than that in the A1 line. Transgene expression was observed not only in the gastrocnemius and quadriceps but also in other areas of skeletal muscle including the tibialis anterior, extensor digitorum longus (EDL), and soleus (not shown). The blot was then re-hybridized with a cDNA probe of Gadd45α, an authentic target gene of FOXO1 (51, 52). As expected, induction of the expression of Gadd45α was observed in skeletal muscle but not in other tissues in both FOXO1 transgenic mouse lines (Fig. 1*C*), indicating that the transgene expressed a functional FOXO1 protein. By using an antibody that recognizes both human and mouse FOXO1, we confirmed

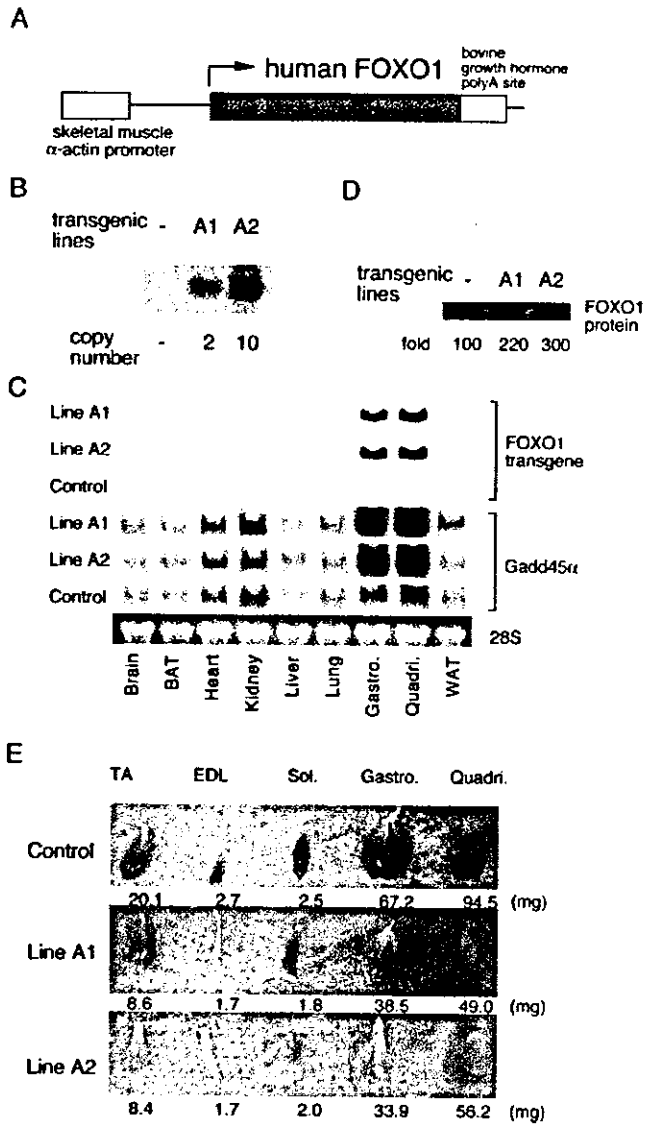

FIG. 1. **Creation of FOXO1 transgenic mice.** *A*, map of the 5-kb construct used for transgenic microinjection. The transgene was under the control of the human skeletal muscle α-actin promoter and included exon 1 and the intron of the human skeletal muscle α-actin gene as well as the bovine growth hormone polyadenylation site (45). *B*, characterization of FOXO1 mice. Two transgenic lines, *A1* and *A2*, were identified by Southern blot analyses of DNA obtained from the tail of each mouse. The copy number was 2 for *A1* and 10 for *A2*, as estimated by densitometric scanning of the autoradiographs of the Southern blot. *C*, expression of the *FOXO1* transgene in mice. Northern blot analysis of human FOXO1 mRNA expression in tissues from FOXO1 mice (*line A1* and *A2*) and nontransgenic control mice. RNAs from brain, brown adipose tissue (*BAT*), heart, kidney, liver, lung, skeletal muscle (gastrocnemius (*Gastro.*) and quadriceps (*Quadri.*)), and white adipose tissue (*WAT*) were analyzed. The blots were re-hybridized with the *Gadd45α* probe. Each lane contained 20 μg of total RNA. *28 S* ribosomal RNA staining of a sample from control mice is shown. Similar staining was observed in samples from transgenic mice (not shown). *D*, expression of the FOXO1 protein in the skeletal muscle of FOXO1 mice. Protein extracts (30 μg per lane) were subjected to SDS-PAGE. The FOXO1 protein was detected by immunoblotting. The densitometric ratio is shown below the autoradiogram (the control was set as *100*). *E*, comparison of representative samples of dissected skeletal muscle (*TA*, tibialis anterior; *Sol*, soleus; *Gastro*, gastrocnemius; *Quadri*, quadriceps) between FOXO1 mice and littermate control mice. Legs were removed from 4-month-old (*lines A1* and *A2*) transgenic mice and age-matched control mice. Tibialis anterior, gastrocnemius, and quadriceps contain a mixture of type I and II fibers; EDL is enriched in type II fibers, and soleus is enriched in type I fibers (control). Average dry mass ($n = 3$ in each group) is shown below the panel. Muscles were smaller in size and paler in color in FOXO1 mice than in control mice.

TABLE I

FOXO1 mice are smaller in body weight and lean body mass

FOXO1 mice weighed less (body weight and lean body mass) than nontransgenic, age- and sex-matched controls, when measured at 5 months of age (line A1) and at 4 months of age (line A2). Fat content per body weight of control and FOXO1 mice did not differ significantly. Data on both male and female mice are shown. Food intake and blood analyses of these mice are also shown. Values represent means ± S.E.

Mice	Numbers	Sex	Age	Body weight	Lean body mass	Fat content	Food intake	Free fatty acid	Lactate	Glucose	Insulin
				g	*g*	%	*g/g/day*	*mEq/liter*	*mg/ml*	*mg/dl*	*pg/ml*
Control	4	Male	5 months	29.0 ± 1.0	24.1 ± 0.3	20.8 ± 1.6	0.18 ± 0.005	0.30 ± 0.025	53.0 ± 4.3	163 ± 2.9	1775 ± 700
A1	4	Male		24.5 ± 0.4[a]	20.3 ± 0.4[b]	20.8 ± 0.5	0.17 ± 0.004	0.34 ± 0.098	56.3 ± 8.3	173 ± 14	739 ± 139
Control	4	Female		21.6 ± 0.9	19.3 ± 0.9	12.9 ± 1.0	0.25 ± 0.017	0.39 ± 0.060	32.7 ± 3.1	158 ± 8.0	289 ± 14
A1	6	Female		18.4 ± 0.4[a]	16.4 ± 0.2[a]	15.8 ± 1.2	0.24 ± 0.017	0.38 ± 0.049	38.9 ± 2.5	163 ± 5.3	302 ± 5
Control	4	Male	4 months	24.3 ± 0.4	21.0 ± 0.4	15.2 ± 1.2	0.21 ± 0.011	0.40 ± 0.045	37.3 ± 3.7	160 ± 10	373 ± 19
A2	4	Male		19.4 ± 0.1[b]	17.4 ± 0.2[b]	15.0 ± 1.9	0.18 ± 0.017	0.33 ± 0.077	46.4 ± 6.6	184 ± 14	573 ± 109
Control	4	Female		19.9 ± 0.6	17.6 ± 0.7	12.8 ± 0.2	0.25 ± 0.027	0.45 ± 0.055	34.5 ± 1.9	144 ± 10	283 ± 10
A2	4	Female		17.3 ± 0.3[a]	15.1 ± 0.4[c]	13.3 ± 0.9	0.23 ± 0.041	0.58 ± 0.096	35.7 ± 5.9	143 ± 6.5	316 ± 10

[a] $p < 0.01$.
[b] $p < 0.001$.
[c] $p < 0.05$.

the presence of the FOXO1 protein in the skeletal muscle of FOXO1 mice (Fig. 1*D*). An ~2.2-fold (line A1) and 3-fold (line A2) increase in FOXO1 protein levels was observed. These increases were at the physiological level, since 24-h fasting has been shown to increase FOXO1 protein content by 2.5–3-fold (Ref. 53 and data not shown).

FOXO1 Mice Are Small—The apparent phenotype observed in FOXO1 mice was small stature and thinner legs than the control mice. Both male and female transgenic mice weighed about 10% less than the control mice at 5 weeks of age (not shown). We used DEXA to measure the lean body mass (body weight excluding fat weight) and the content of fat in the whole body of the A1 line (at 5 months of age) and the A2 line (at 4 months of age) in age- and sex-matched control mice (Table I). Both body weight and lean body mass were significantly lower in both male and female FOXO1 mice (both lines) than in control mice. However, the fat content per total body weight of both FOXO1 mouse lines was comparable with that of nontransgenic mice (Table I). Thus, the decrease in body weight of the FOXO1 mice is not caused by a decrease in body fat but by a decrease in lean body mass. Consistent with the data on decreased lean body mass, the skeletal muscles in FOXO1 mice were smaller in size and dry mass, as well as paler in color than those of control mice (Fig. 1*E*). Consumption of food per body weight was not significantly different between FOXO1 mice and control mice (Table I). Blood metabolite (free fatty acid, lactate, and glucose) and insulin levels did not differ significantly between FOXO1 mice and the controls (Table I).

Microarray Analysis—To obtain information on changes in gene expression in FOXO1 mice, we performed microarray analysis using RNA samples from skeletal muscle (quadriceps) of transgenic and control mice. Most interestingly, the largest category of genes with suppressed expression in the transgenic mice was those involved in cell structure. Namely, about half of the down-regulated genes were classified as cytoskeletal proteins (Table II). The FOXO1-induced genes were distributed throughout various categories (not shown, see Supplemental Material 1).

In the skeletal muscle of FOXO1 mice, there was a decrease in the expression levels of genes related to structural proteins of the type I fiber (slow twitch oxidative, red muscle), such as slow muscle isoforms of myosins (Table II, line numbers 1, 4, and 6), slow isoforms of troponins (Table II, line numbers 2, 5, and 7), α-tropomyosin slow type (Table II, line number 13), myoglobin (Table II, line number 12), and mtCK (Table II, line number 15), which are abundant in type I fibers (54). This is consistent with the observation that the skeletal muscles of FOXO1 mice are pale (Fig. 1*E*). In the microarray, the expression of mitochondrial oxidative metabolism genes, such as the electron transport system, did not differ between FOXO1 mice and controls (not shown). In large mammals such as humans, type I fibers are higher in mitochondrial content and more dependent on oxidative metabolism than type II fibers. In small mammals (*e.g.* mouse and rat), a large amount of mitochondria is seen in type II fibers as well as type I fibers (2). The large amount of mitochondria in both type I and type II fibers in mice would explain the unchanged gene expression of the mitochondrial electron transport system, although expression of type I fiber genes was markedly suppressed. In addition, the gene expression of type II fiber isoforms did not differ (not shown). Namely, expression of genes preferentially abundant in type I fibers appears to be suppressed in the skeletal muscle of FOXO1 mice.

Northern Blot Analysis of Representative Genes—We recognize the limitation of single microarray assays, as they can contain certain noise in the data. Thus, to verify the changes of gene expression found in the microarray analysis, we performed Northern blot analysis by using probes for several genes. In addition to representative genes in the list (Table II), we also analyzed several additionally selected genes of type I fiber or type II fiber markers or genes that may be involved in fiber differentiation. FOXO1 overexpression did not significantly affect mRNA levels of the other FOXO members, FOXO4 and FOXO3a (Fig. 2*A*). Consistent with the microarray data, a reduction in gene expression was confirmed for type I fiber proteins, such as troponin C (slow) (Table II, line number 2), MLC (slow) (Table II, line number 6), troponin T (slow) (Table II, line number 7), myoglobin (Table II, line number 12), and mtCK (Table II, line number 15) (Fig. 2*A*). On the other hand, expression levels of genes for components of the mitochondrial electron transport system, such as cytochrome *c* oxidase II and IV (COX II and IV), and the F_0F_1-ATPase, were not markedly changed in the skeletal muscle of FOXO1 mice. Next, we examined type II fiber genes. The expression of genes for troponin I (fast), troponin T (fast), and MLC (fast) did not differ between FOXO1 mice and control mice. Thus, the results of the microarray analysis were confirmed by Northern blot analysis. In addition, given that Mef2, NFAT, CaMK, and PGC-1α have been implicated recently in regulating gene expression in type I fibers (14–18, 22), we also examined the level of their expression in skeletal muscle of control and FOXO1 mice. PGC-1α mRNA levels were slightly increased in the skeletal muscle of FOXO1 mice (line A2). Most interestingly, expression levels of Mef2c and CaMK were reduced in FOXO1 mice. FOXO1-mediated down-regulation of type I fiber genes may, in part, be regulated by Mef2c and CaMK.

Moreover, we examined the expression levels of genes whose expression levels are known to be changed during skeletal

TABLE II

Gene with decreased expression in the skeletal muscle of FOXO1 mice

The expression levels of 22 genes were significantly decreased in both the A1 and A2 lines of FOXO1 mice. The genes are listed in the order of greatest fold change in expression in skeletal muscle from line A1 mice relative to control mice. Fold change calculations were carried out as an indication of the relative change of each transcript represented on the probe array. The average difference value is a marker of abundance of each gene. Categories and subcategories are based on a previously established classification scheme (50) and literature review. Change (↓) indicates that expression is significantly decreased compared with control mice.

	GenBank™ accession no.	Gene description	Categories	Subcategories	Fold change (line A1)	Fold change (line A2)	Average difference (control)	Average difference (line A1)	Average difference (line A2)
1	AJ223362	Myosin, heavy polypeptide 7, cardiac muscle, β	Cell structure	Cytoskeletal	−57.6 ↓	−41.8 ↓	418	−97	10
2	M29793	Troponin C (cardiac/slow skeletal isoform)	Cell structure	Cytoskeletal	−30.4 ↓	−9.7 ↓	260	2	39
3	U88623	Aquaporin 4	Metabolism	Transport	−21 ↓	−10.2 ↓	259	10	21
4	X12972	Myosin alkali light chain (ventricular/slow muscle isoform)	Cell structure	Cytoskeletal	−6.8 ↓	−2.1 ↓	937	129	450
5	AJ242874	Troponin I, skeletal, slow 1	Cell structure	Cytoskeletal	−6.7 ↓	−3.2 ↓	313	48	109
6	M91602	Myosin light chain 2 (cardiac ventricle isoform)	Cell structure	Cytoskeletal	−5.8 ↓	−3 ↓	1038	165	316
7	AV213431	Troponin T1 (slow twitch isoform)	Cell structure	Cytoskeletal	−4.4 ↓	−3.1 ↓	772	174	246
8	M74570	Aldehyde dehydrogenase II	Metabolism	Sugar/glycolysis	−4 ↓	−2.8 ↓	567	140	209
9	U34277	Platelet-activating factor acetylhydrolase	Cell defense	Homeostasis	−3.1 ↓	−2 ↓	238	77	120
10	AI646638	Clone MGC:37615 IMAGE: 4989784, mRNA,	Not found in the list		−2.9 ↓	−2.2 ↓	150	51	68
11	D45203	Pentylenetetrazole-related mRNA PTZ-17	Not found in the list		−2.8 ↓	−3 ↓	1232	434	411
12	X04405	Myoglobin	Cell defense	Homeostasis	−2.8 ↓	−1.8 ↓	2484	812	1410
13	U04541	Tropomyosin 3 (slow twitch isoform)	Cell structure	Cytoskeletal	−2.7 ↓	−2.4 ↓	662	243	273
14	X92665	Ubiquitin-conjugating enzyme E2E1	Protein expression	Post-translational modification	−2.1 ↓	−1.7 ↓	298	187	175
15	AV250974	Creatine kinase, mitochondrial 2	Metabolism	Sugar/ glycolysis	−2 ↓	−1.8 ↓	671	300	339
16	X57349	Transferrin receptor	Cell defense	Homeostasis	−1.9 ↓	−2.8 ↓	276	121	82
17	L12447	Insulin-like growth factor-binding protein 5	Unclassified		−1.9 ↓	−1.9 ↓	2080	1111	1095
18	Z38015	Myotonin protein kinase	Cell signaling	Protein modification	−1.9 ↓	−1.8 ↓	684	361	374
19	AB010144	Mitsugumin29, a synaptophysin family	Cell structure	General	−1.8 ↓	−2.4 ↓	742	414	312
20	X63615	Calcium/calmodulin-dependent protein kinase II, β	Cell signaling	Protein modification	−1.8 ↓	−2.1 ↓	295	160	146
21	U00677	Syntrophin, acidic 1	Cell structure	Cytoskeletal	−1.7 ↓	−1.7 ↓	857	504	491
22	AF032099	Potassium voltage-gated channel	Cell signaling	Channel/transport	−1.5 ↓	−1.6 ↓	320	209	195

muscle atrophy such as caused by fasting, cachexia, and STZ-induced diabetes (55). Specifically, gene expression of atrogin 1/MAFbx, MuRF1 (both are ubiquitin ligases), and cathepsin L (a lysosomal protease) is up-regulated and IGFBP5 is down-regulated during skeletal muscle atrophy (55). In our Northern blot analysis, the level of atrogin 1 expression was increased in the A2 line of FOXO1 mice, which has less skeletal muscle, but not in the A1 line, which also has less skeletal muscle mass than nontransgenic controls. In both the A1 and A2 lines of FOXO1 mice, the expression of cathepsin L and IGFBP5 was increased and decreased, respectively. The MuRF1 mRNA level was not changed. Thus, atrophy-related gene expression changes including that of protein degradation likely occurred in the skeletal muscle of FOXO1 mice.

Western Blot Analysis of the Skeletal Muscle of FOXO1 Mice and PGC-1α Mice—We examined the expression of various gene products of FOXO1 mice at the protein level by Western blot analysis (Fig. 2*B*). Protein extracts from the skeletal muscle of FOXO1 mice (A1 and A2 lines) and wild-type control mice were used. For comparison, we analyzed protein extracts from the skeletal muscle of PGC-1α transgenic mice, which we previously analyzed (23). Protein levels of troponin I (slow) and myoglobin, which are rich in type I fibers, were increased in PGC-1α mice but decreased in FOXO1 mice (Fig. 2*B*). On the other hand, the protein level of troponin I (fast), which is rich in type II fibers, was decreased in PGC-1α mice but not in FOXO1 mice (Fig. 2*B*). Thus, Western blot analysis of the protein expression of genes for type I and type II fibers was consistent with the results of mRNA expression analysis.

Histological Analysis of Skeletal Muscle of FOXO1 Mice—We examined the relationship between the change in type I fiber gene expression and actual muscle fiber morphology in the skeletal muscle (soleus) of transgenic mice using light microscopy and histochemical procedures (A1 line, 4 months after birth; A2 line, 3 months after birth). Distinction between type I and type II fibers can be made by myosin ATPase staining at different pH values. Specifically, at pH 10.5, type II fibers are well stained but not type I fibers, and at pH 4.3, type I fibers are well stained but not type II fibers (2). ATPase staining revealed that skeletal muscle cells (both type I and type II fibers) in the FOXO1 mice are smaller than those of the control mice (average cross-sectional area of muscle fibers; A1 line, 11.5 ± 0.8 μm^2 in FOXO1 mice and 20.0 ± 2.7 μm^2 in control mice; A2 line, 9.8 ± 0.5 μm^2 in FOXO1 mice and 14.1 ± 1.9 μm^2 in control mice) and had fewer type I fibers than those in the control mice (average; A1 line, 28.6 ± 1.3% in FOXO1 mice and

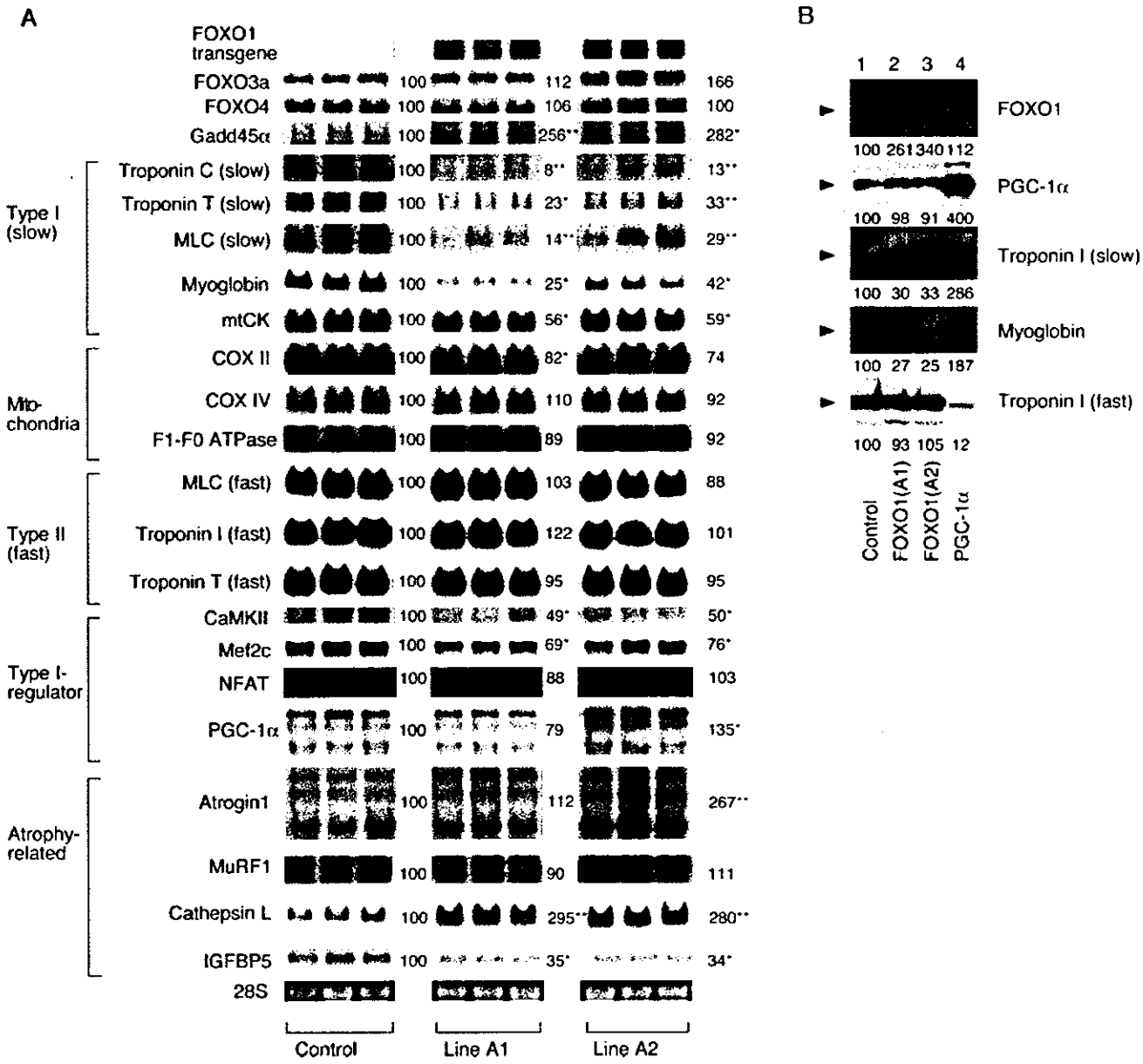

FIG. 2. **Gene product levels in the skeletal muscle of FOXO1 mice.** *A*, Northern blot analysis was performed on total RNA (20 μg per lane) isolated from skeletal muscle (quadriceps) of FOXO1 mice (*line A1* and *line A2*) and nontransgenic control mice. The same RNA sample sets were blotted onto multiple membranes and hybridized with the indicated probes. The names of genes examined are on the *left* of the autoradiograms, and average densitometric ratios (the control was set as *100*) are on the *right* (*, $p < 0.05$; **, $p < 0.01$). Equal sample loading was confirmed by ethidium bromide staining of 28 S ribosomal RNA. Each lane represents a sample from an individual mouse. *B*, Western blot analysis was performed on protein extracts from the skeletal muscle of *FOXO1* mice (*A1* and *A2* lines), PGC-1α mice, and control mice. Antibodies against FOXO1, PGC-1α, troponin I (slow), myoglobin, and troponin I (fast) were used. A typical autoradiogram, representative of three independent experiments with similar results, is shown. *Numbers* below the panels are values of the densitometric ratios (the signal of the control for each sample was set as *100*). Corresponding bands are indicated by *arrowheads*. The approximate estimated molecular sizes are as follows: FOXO1, 70 kDa; PGC-1α, 90 kDa; troponin I (slow), 30 kDa; myoglobin, 30 kDa; and troponin (fast), 40 kDa.

37.8 ± 2.2% in control; A2 line, 20.2 ± 2.3% in FOXO1 mice and 40.4 ± 2.0% in control) (Fig. 3*A*). Immunohistochemistry with antibodies to myoglobin (present at high concentrations in type I fibers) confirmed the reduction in the number of type I fibers in the skeletal muscle of FOXO1 mice (not shown). Skeletal muscle samples from FOXO1 mice had no structural abnormalities such as mitochondrial abnormalities, glycogen accumulation, vacuolar formation, and muscle fiber degeneration (not shown).

Running Wheel Activity of FOXO1 Mice—The mass and fiber composition of skeletal muscle are important for physical exercise. Type I fibers are more resistant to fatigue than type II fibers (2). As the FOXO1 mice had decreased total skeletal muscle mass and fewer type I fibers, they may have a low capacity for endurance, such as that needed in a marathon. We then compared the running wheel activity (spontaneous locomotive activity) in FOXO1 mice and control mice. Mice were transferred to cages with a running wheel and monitored daily for the number of wheel revolutions made for 6 days. Both lines of FOXO1 mice showed significantly fewer wheel revolutions (Fig. 3*B*). The decrease in running wheel activity suggested that FOXO1 mice were less able to sustain continuous muscle

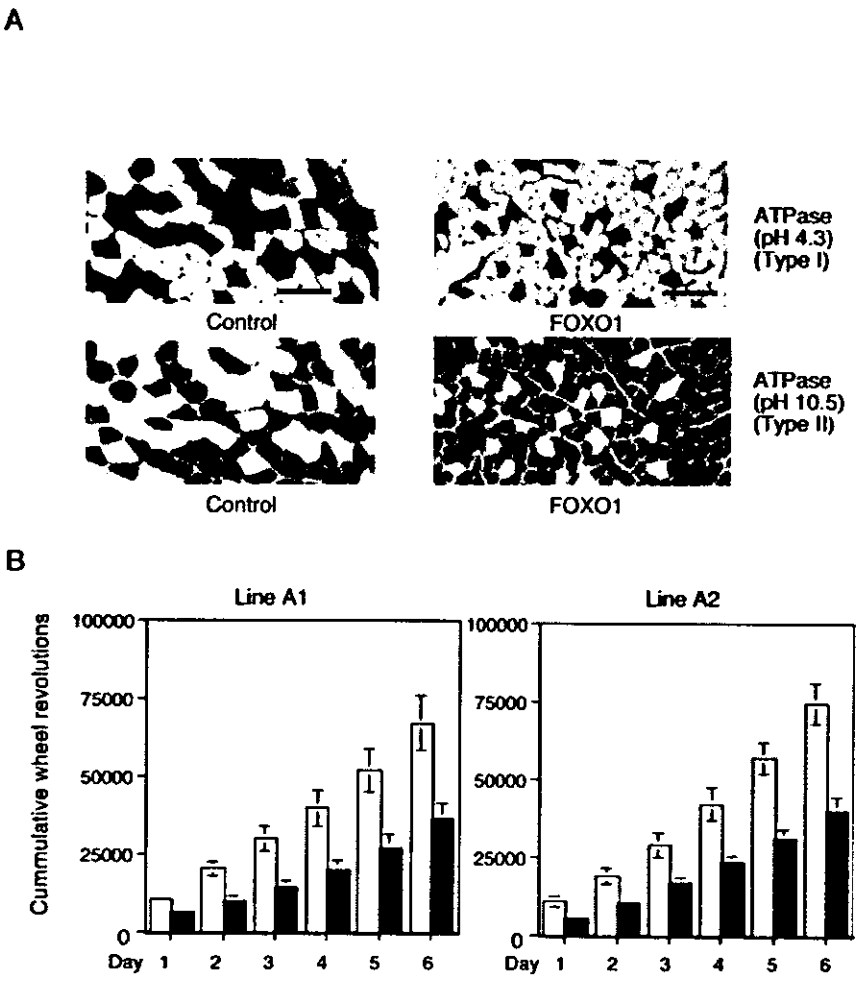

FIG. 3. *A*, histological analysis of skeletal muscle. Light microscopy of ATPase (pH 4.3 for type I fibers and pH 10.5 for type II fibers)-stained transverse sections of skeletal muscle (soleus) specimens from FOXO1 mice (line A2) and control littermates at 3 months of age. *Bars*, 50 μm. Skeletal muscle fibers of *FOXO1* mice were thinner and contained fewer type I fibers than that of control mice. *B*, running wheel activity of FOXO1 mice. Mice were housed individually in cages equipped with a running wheel (20 cm in diameter). The number of revolutions made was recorded daily for 6 days, and the cumulative values are shown. *Open column*, control; *closed column*, FOXO1 mice. Running wheel activity was significantly ($p < 0.05$) reduced in FOXO1 mice (*line A1*, *left*; *line A2*, *right*) compared with control mice. Mice used were females at 10 weeks (*line A1*) and 9 weeks (*line A2*) of age. Numbers of animals used are as follows: line A1, control, $n = 6$; FOXO1 mice, $n = 5$; line A2, control, $n = 4$; FOXO1 mice, $n = 3$. Because male mice responded similarly, only the data from female mice are shown. *C* and *D*, oral glucose tolerance tests (*C*) and insulin tolerance tests (*D*) on FOXO1 mice. For the oral glucose tolerance test, mice were fasted overnight and given D-glucose (1 mg/g body weight) orally by a stomach tube. Blood glucose levels were determined at the times indicated. For the insulin tolerance test, mice were allowed free access to food and then given 0.75 milliunits of human insulin/g of body weight. Blood glucose levels were measured at the indicated time points. Mice used were males at 10 weeks (line A1) and 9 weeks (line A2) of age. The numbers of animals used were: *line A1*, control, $n = 6$; FOXO1 mice, $n = 5$; *line A2*, control, $n = 5$; FOXO1 mice, $n = 4$.

contractions than control mice, which is consistent with the reduction in the mass of skeletal muscle and the number of type I fibers.

Oral Glucose Tolerance Test and Insulin Tolerance Test on FOXO1 Mice—Skeletal muscle is important for glucose metabolism. To examine whether the decreased skeletal muscle mass of FOXO1 mice is affecting their systemic glucose homeostasis, we examined oral glucose tolerance and insulin tolerance in FOXO1 mice. Glucose tolerance was impaired in both lines of FOXO1 mice, namely peak blood glucose values in FOXO1 mice were elevated significantly above those of the control mice (Fig. 3*C*). The insulin tolerance test clearly demonstrated that the glucose-lowering effects of insulin were impaired in both the A1 and A2 lines of FOXO1 mice, compared with those in age- and sex-matched control mice (Fig. 3*D*). FOXO1 mice showed a low capacity for glucose metabolism and decreased insulin sensitivity. Adipose tissue, another organ playing a role in glucose metabolism, appears not to be involved in this impaired glycemic control because 1) body fat did not differ between FOXO1 mice and control mice (Table I), and 2) gene expression of glucose transporter 4, which is a rate-limiting molecule of insulin-dependent glucose intake (56), was not decreased in adipose tissue of FOXO1 mice (see Supplemental Material 2). FOXO1 mice may therefore represent a certain type of diabetic state in humans.

Change in Endogenous FOXO1 Expression by Physical Inactivity—We performed Northern blot analysis with RNA from the skeletal muscle of mice maintained under a long period of physical inactivity. The right hindlimbs of wild-type mice were immobilized in plaster casts, and the left hindlimbs were left freely moving for the control sample. After 3 weeks in the plaster casts, skeletal muscle (gastrocnemius) weight of the right hindlimbs was significantly decreased compared with that in the controls (average, 88 ± 12 mg for immobilized and 149 ± 6 mg for freely moving controls, $n = 3$, $p < 0.05$). As shown in Fig. 4, the gene expression of troponin C (slow), myoglobin, and mtCK but not MLC (fast) and troponin T (fast) was markedly decreased in the plaster-casted muscle. At the same time, endogenous FOXO1 mRNA was increased in the immobilized muscle (Fig. 4). Furthermore, Gadd45α was increased in the same sample. In addition, cathepsin L, but not atrogin 1 and MuRF1, were increased (Fig. 4). Thus, mRNAs of endogenous FOXO1, Gadd45α, and cathepsin L were increased; skeletal muscle mass was decreased, and the expression of type I fiber genes but not type II fiber genes were decreased. The gene expression changes observed in the plaster-casted skeletal muscle were similar to the changes observed in the FOXO1 mice (Fig. 2*A*). These results further support the involvement of FOXO1 in the negative regulation of skeletal muscle mass and the expression of type I fiber genes.

DISCUSSION

To gain insight into the role of FOXO1 in skeletal muscle *in vivo*, we established transgenic mice overexpressing human FOXO1. The *FOXO1* transgene was predominantly expressed in the skeletal muscle, and the increase in FOXO1 protein expression was within physiological levels. Most interestingly, the skeletal muscle of FOXO1 mice weighed less and was paler

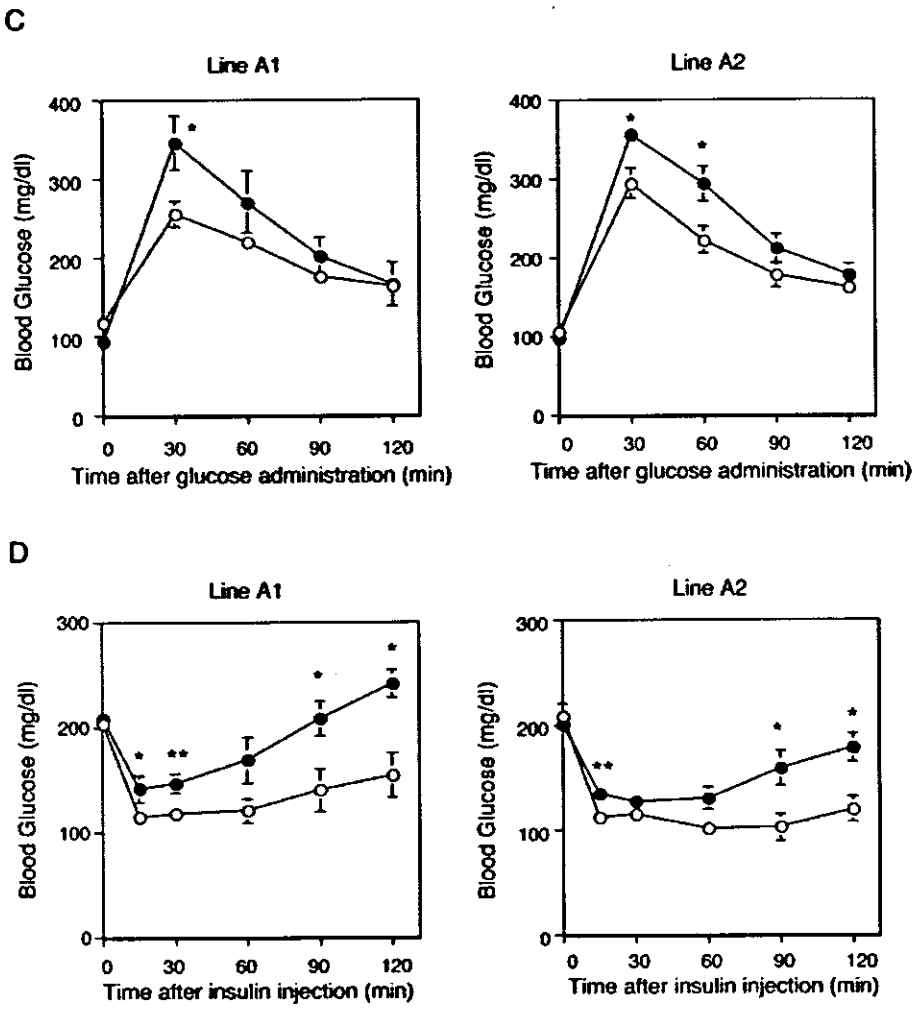

FIG. 3—*continued*

in color. The results of gene expression analyses showed that type I (red muscle) fiber-related gene expression was decreased in the skeletal muscle of FOXO1 mice. In addition, histological examinations showed that the skeletal muscle of FOXO1 mice had fewer type I fibers and smaller type I and type II fibers. Consistently, under long time physical inactivity by immobilizing skeletal muscle in plaster casts, an increased expression of endogenous FOXO1 mRNA and a markedly decreased expression of genes related to type I fibers were observed. These results suggest that FOXO1 is a negative regulator of skeletal muscle mass and expression of type I fiber-related genes. Moreover, FOXO1 mice showed poor glycemic control and low capacity for physical exercise, which involves the skeletal muscles, especially type I fibers. These phenotypes are consistent with the decreased mass of skeletal muscle including type I fibers in FOXO1 mice.

How does FOXO1 affect the skeletal muscle, including the reduction of mass of both type I and type II fibers and the suppressed expression of type I fiber genes? In the following, we discuss the possibility of involvement of FOXO1 in 1) growth, 2) protein degradation, and 3) differentiation of skeletal muscle.

1) FOXO1 may suppress increase of skeletal muscle mass. A genetic study of *C. elegans* showed that DAF16, the worm counterpart of FOXO, functions as a suppressor of insulin receptor-like signaling (44). Thus, the FOXO family might act negatively in mammals as a downstream player in insulin or IGF signaling. IGF-1 stimulates the proliferation of skeletal muscle satellite cells (57). Mature skeletal muscle fibers are not able to proliferate. Skeletal muscle satellite cells, mononuclear cells located between the basement membrane and the plasma membrane of myofibers in mature cells, are important in postnatal skeletal muscle hypertrophy because of their ability to add new myonuclei into growing myofibers. Machida *et al.* (58) showed that FOXO1 inhibited IGF-1-mediated skeletal muscle cell proliferation. In primary skeletal muscle satellite cells, FOXO1 activates the promoter of p27 Kip1, an inhibitor of the cell cycle at the G_1 stage, which leads to inhibition of cell proliferation, and addition of IGF-1 reverses the FOXO1-mediated activation of the p27 Kip1 promoter (58). Unexpectedly, p27 Kip1 mRNA expression was unchanged in the skeletal muscle of FOXO1 mice compared with that of controls (not shown). As the ratio of satellite cells is very small in total skeletal muscle, the increased expression of p27 Kip1 in satellite cells may not have been detected in our assay. On the other hand, we showed enhanced expression of Gadd45α, an inhibitor of the cell cycle at the G_2 stage (51, 52), in the skeletal muscle of FOXO1 mice (Figs. 1 and 2A). As a 0.7-kb stretch of the rat skeletal muscle α-actin promoter is active in skeletal muscle satellite cells (59), the *FOXO1* transgene, driven by a 2-kb stretch of the human skeletal muscle α-actin promoter (45), is likely to be expressed in the skeletal muscle satellite cells of the FOXO1 mice. Thus, the increased amount of Gadd45α and possibly p27 Kip1 in the skeletal muscle satellite cells of FOXO1 mice may have suppressed the proliferation of satellite cells and caused a decrease in skeletal muscle mass (size).

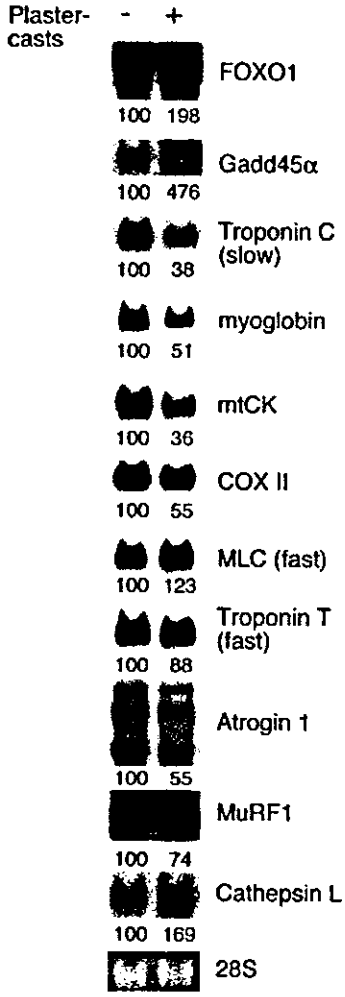

FIG. 4. **Gene expression in skeletal muscle immobilized in plaster casts.** The right hindlimbs of mice at 9 weeks of age were immobilized in plaster casts, and left hindlimbs of the mice were kept free for the control sample. After 3 weeks of immobilization in plaster casts, Northern analysis was performed on total RNA (20 μg per lane) isolated from the skeletal muscle (gastrocnemius) of right hindlimbs and left hindlimbs. *Plus* and *minus* denote with or without immobilization, respectively. The names of the genes examined are on the *right* of the autoradiograms. A typical autoradiogram, representative of three independent mice with similar results, is shown. The densitometric ratio is shown *below* the autoradiograms (the control was set as *100*).

2) FOXO1 may increase the degradation rate of skeletal muscle proteins. Gene expression of atrogin 1, MuRF1 (both are ubiquitin ligases), and cathepsin L (a lysosomal protease) is up-regulated and IGFBP5 is down-regulated during skeletal muscle atrophy caused by fasting, cachexia, STZ-induced diabetes, and other diseases (55). After we submitted our manuscript, a member of the FOXO family, FOXO3a, was reported to activate the gene expression of atrogin 1, and addition of IGF-1 was found to reverse the FOXO3a-mediated activation of the atrogin 1 promoter (60). Overexpression of an active form of FOXO3a reduces the size of skeletal muscle fibers, both *in vivo* and *in vitro* (60). In addition, another group reported that overexpression of an active form of FOXO1 in C2C12 muscle cells did not change the base-line expression of atrogin 1 and MuRF1, but the active form of FOXO1 suppresses IGF-1-mediated repression of atrogin 1 and MuRF1 expression induced by glucocorticoids (61). This suggests that FOXO1 expression is not sufficient for inducing atrophy-related genes, but FOXO1 is negatively involved in IGF-1-mediated suppression of atrophy of skeletal muscle. In our Northern blot analysis, the level of atrogin 1 was increased in the A2 line but not in the A1 line of FOXO1 mice, although both had less skeletal muscle mass than the nontransgenic controls. In both the A1 and A2 lines of FOXO1 mice, the expression of cathepsin L and IGFBP5 was increased and decreased, respectively. MuRF1 mRNA levels were not altered in both lines. Thus, atrophy-related protein degradation probably occurs in the skeletal muscle of FOXO1 mice and could explain, in part, the decrease in skeletal muscle mass of the FOXO1 mice. However, the increase in atrogin 1 is unlikely to be enough to cause the decrease in skeletal muscle mass of FOXO1 mice, because the expression level did not change in the A1 line of FOXO1 mice. This is consistent with the description by Sandri *et al.* (60) that overexpression of atrogin 1 alone does not cause myotube or muscle atrophy. On the other hand, IGFBP5 is reported to modulate the activity of IGF-1 (62), and hence decreased expression of IGFBP5 may contribute to the decrease in skeletal muscle mass by affecting IGF-1 action. *FOXO1* transgene expression was observed in both type I fiber-rich soleus and type II fiber-rich EDL. Thus, changes in the expression of atrophy-related genes may be an alternative molecular explanation for the decreased skeletal muscle mass, including the size of both type I and type II fibers of FOXO1 mice.

3) Does FOXO1 inhibit the differentiation of type I fibers? The *FOXO1* transgene is expressed in muscles rich in both type I and type II fibers. How does it cause the selective reduction of gene expression in type I fibers but not in type II fibers? It is possible that FOXO1 suppresses the function of a factor(s) that is preferentially expressed in type I fibers and therefore activates gene expression only in type I fibers. One candidate for such a factor is PGC-1α, which is known to be preferentially expressed in type I fibers and enhances type I fiber gene expression (22). As the FOXO1 protein can interact with the PGC-1α protein (43), FOXO1 may affect certain functions of PGC-1α. FOXO1 may inhibit PGC-1α function via its binding to PGC-1α. FOXO1 itself is a transcription factor. In addition, several reports (27–30) have shown that FOXO1 acts as a corepressor of nuclear receptors, whereas PGC-1α can activate many nuclear receptors (21, 63). Although to our knowledge nuclear receptors have not been shown to be involved in type I fiber-specific gene expression, a certain nuclear receptor(s) and transcription factor(s), which can interact with both FOXO1 and PGC-1α, may be involved in a process positively and negatively regulated by PGC-1α and FOXO1, respectively. Further studies are required to examine this possibility. Besides, although PGC-1α stimulates the differentiation of type I fibers, in FOXO1 mice, gene expression was reduced in type I fibers but was not affected in type II fibers. Thus, fiber differentiation (switching) from type I to type II is not likely to occur in FOXO1 mice, and FOXO1 appears not to be involved in fiber differentiation.

Calcineurin (14, 17) and CaMK (15), downstream molecules of calcium signaling (13), the transcription factors Mef2c (14–16, 18) and NFAT (14, 15, 17), as well as the nuclear receptor coactivator PGC-1α (22) are known to promote type I fiber differentiation and type I fiber gene expression. In skeletal muscle of FOXO1 mice, mRNA levels of Mef2c and CaMK are significantly decreased (Fig. 2*A*). FOXO1 may reduce gene expression in type I fiber by suppressing gene expression of Mef2c and CaMK.

FOXO1 mice showed a clear phenotype related to the function of skeletal muscle. Specifically, spontaneous locomotor activity was lower in FOXO1 mice than in control mice (Fig. 3*B*). In addition, FOXO1 mice had impaired oral glucose tolerance and impaired insulin-mediated glucose-lowering effects (Fig. 3, *C* and *D*). Elderly humans have been reported to show

a progressive loss of muscle fibers associated with diabetes, obesity, and decreased physical activity (sarcopenia). Overexpression of IGF-1 in skeletal muscle prevents the age-related decline in muscle mass (11, 57). As described above, the reduced skeletal muscle mass in FOXO1 mice may be caused by the suppression of IGF signaling during skeletal muscle formation, and FOXO1 may therefore be involved in age-related sarcopenia in humans. FOXO1 mice may be valuable as a model for human diseases related to loss of muscle fibers. Further analysis of the molecular mechanisms of FOXO1 action in skeletal muscle is important from a clinical as well as a sports science perspective.

Acknowledgments—We thank H. Meguro for technical assistance, Dr. S. Machida (University of Missouri, Columbia) for valuable comments, and Dr. H. A. Popiel for proofreading.

REFERENCES

1. Zurlo, F., Larson, K., Bogardus, C., and Ravussin, E. (1990) *J. Clin. Investig.* **86,** 1423–1427
2. Berchtold, M. W., Brinkmeier, H., and Muntener, M. (2000) *Physiol. Rev.* **80,** 1215–1265
3. Proctor, D., Balagopal, P., and Nair, K. (1998) *J. Nutr.* **128,** S351–S355
4. Fitts, R., Riley, D., and Widrick, J. (2001) *J. Exp. Biol.* **204,** 3201–3208
5. Hickey, M. S., Carey, J. O., Azevedo, J. L., Houmard, J. A., Pories, W. J., Israel, R. G., and Dohm, G. L. (1995) *Am. J. Physiol.* **268,** E453–E457
6. Gaster, M., Staehr, P., Beck-Nielsen, H., Schroder, H. D., and Handberg, A. (2001) *Diabetes* **50,** 1324–1329
7. Tanner, C. J., Barakat, H. A., Dohm, G. L., Pories, W. J., MacDonald, K. G., Cunningham, P. R., Swanson, M. S., and Houmard, J. A. (2002) *Am. J. Physiol.* **282,** E1191–E1196
8. Frost, R. A., and Lang, C. H. (2003) *Minerva Endocrinol.* **28,** 53–73
9. DeVol, D., Rotwein, P., Sadow, J., Novakofski, J., and Bechtel, P. (1990) *Am. J. Physiol.* **259,** E89–E95
10. Zdanowicz, M., Moyse, J., Wingertzahn, M., O'Connor, M., Teichberg, S., and Slonim, A. (1995) *Endocrinology* **136,** 4880–4886
11. Barton-Davis, E. R., Shoturma, D. I., Musaro, A., Rosenthal, N., and Sweeney, H. L. (1998) *Proc. Natl. Acad. Sci. U. S. A.* **95,** 15603–15607
12. Florini, J., Ewton, D., and Coolican, S. (1996) *Endocr. Rev.* **17,** 481–517
13. Stull, J. T. (2001) *J. Biol. Chem.* **276,** 2311–2312
14. Chin, E. R., Olson, E. N., Richardson, J. A., Yang, Q., Humphries, C., Shelton, J. M., Wu, H., Zhu, W., Bassel-Duby, R., and Williams, R. S. (1998) *Genes Dev.* **12,** 2499–2509
15. Wu, H., Naya, F. J., McKinsey, T. A., Mercer, B., Shelton, J. M., Chin, E. R., Simard, A. R., Michel, R. N., Bassel-Duby, R., Olson, E. N., and Williams, R. S. (2000) *EMBO J.* **19,** 1963–1973
16. Yan, Z., Serrano, A. L., Schiaffino, S., Bassel-Duby, R., and Williams, R. S. (2001) *J. Biol. Chem.* **276,** 17361–17366
17. Chakkalakal, J. V., Stocksley, M. A., Harrison, M. A., Angus, L. M., Deschenes-Furry, J., St-Pierre, S., Megeney, L. A., Chin, E. R., Michel, R. N., and Jasmin, B. J. (2003) *Proc. Natl. Acad. Sci. U. S. A.* **100,** 7791–7796
18. Karasseva, N., Tsika, G., Ji, J., Zhang, A., Mao, X., and Tsika, R. (2003) *Mol. Cell. Biol.* **23,** 5143–5164
19. Kamei, Y., Xu, L., Heinzel, T., Torchia, J., Kurokawa, R., Gloss, B., Lin, S. C., Heyman, R. A., Rose, D. W., Glass, C. K., and Rosenfeld, M. G. (1996) *Cell* **85,** 403–414
20. Glass, C. K., Rose, D. W., and Rosenfeld, M. G. (1997) *Curr. Opin. Cell Biol.* **9,** 222–232
21. Puigserver, P., Wu, Z., Park, C. W., Graves, R., Wright, M., and Spiegelman, B. M. (1998) *Cell* **92,** 829–839
22. Lin, J., Wu, H., Tarr, P. T., Zhang, C. Y., Wu, Z., Boss, O., Michael, L. F., Puigserver, P., Isotani, E., Olson, E. N., *et al.* (2002) *Nature* **418,** 797–801
23. Miura, S., Kai, Y., Ono, M., and Ezaki, O. (2003) *J. Biol. Chem.* **278,** 31385–31390
24. Anderson, M. J., Viars, C. S., Czekay, S., Cavenee, W. K., and Arden, K. C. (1998) *Genomics* **47,** 187–199
25. Kaestner, K. H., Knochel, W., and Martinez, D. E. (2000) *Genes Dev.* **14,** 142–146
26. Galili, N., Davis, R. J., Fredericks, W. J., Mukhopadhyay, S., Rauscher, F. J., 3rd, Emanuel, B. S., Rovera, G., and Barr, F. G. (1993) *Nat. Genet.* **5,** 230–235
27. Schuur, E. R., Loktev, A. V., Sharma, M., Sun, Z., Roth, R. A., and Weigel, R. J. (2001) *J. Biol. Chem.* **276,** 33554–33560
28. Zhao, H. H., Herrera, R. E., Coronado-Heinsohn, E., Yang, M. C., Ludes-Meyers, J. H., Seybold-Tilson, K. J., Nawaz, Z., Yee, D., Barr, F. G., Diab, S. G., Brown, P. H., Fuqua, S. A. W., and Osborne, C. K. (2001) *J. Biol. Chem.* **276,** 27907–27912
29. Dowell, P., Otto, T. C., Adi, S., and Lane, M. D. (2003) *J. Biol. Chem.* **278,** 45485–45491
30. Hirota, K., Daitoku, H., Matsuzaki, H., Araya, N., Yamagata, K., Asada, S., Sugaya, T., and Fukamizu, A. (2003) *J. Biol. Chem.* **278,** 13056–13060
31. Ayala, J. E., Streeper, R. S., Desgrosellier, J. S., Durham, S. K., Suwanichkul, A., Svitek, C. A., Goldman, J. K., Barr, F. G., Powell, D. R., and O'Brien, R. M. (1999) *Diabetes* **48,** 1885–1889
32. Barthel, A., Schmoll, D., Kruger, K. D., Bahrenberg, G., Walther, R., Roth, R. A., and Joost, H. G. (2001) *Biochem. Biophys. Res. Commun.* **285,** 897–902
33. Nakae, J., Kitamura, T., Silver, D. L., and Accili, D. (2001) *J. Clin. Investig.* **108,** 1359–1367
34. Nadal, A., Marrero, P. F., and Haro, D. (2002) *Biochem. J.* **366,** 289–297
35. Dijkers, P. F., Medema, R. H., Pals, C., Banerji, L., Thomas, N. S. B., Lam, E. W. F., Burgering, B. M. T., Raaijmakers, J. A. M., Lammers, J. W. J., Koenderman, L., and Coffer, P. J. (2000) *Mol. Cell. Biol.* **20,** 9138–9148
36. Medema, R. H., Kops, G. J. P. L., Bos, J. L., and Burgering, B. M. T. (2000) *Nature* **404,** 782–787
37. Brunet, A., Bonni, A., Zigmond, M. J., Lin, M. Z., Juo, P., Hu, L. S., Anderson, M. J., Arden, K. C., Blenis, J., and Greenberg, M. E. (1999) *Cell* **96,** 857–868
38. Kops, G. J. P. L., Dansen, T. B., Polderman, P. E., Saarloos, I., Wirtz, K. W. A., Coffer, P. J., Huang, T. T., Bos, J. L., Medema, R. H., and Burgering, B. M. T. (2002) *Nature* **419,** 316–321
39. Nakae, J., Kitamura, T., Kitamura, Y., Biggs, W. H., III, Arden, K. C., and Accili, D. (2003) *Dev. Cell* **4,** 119–129
40. Bois, P. R. J., and Grosveld, G. C. (2003) *EMBO J.* **22,** 1147–1157
41. Nakae, J., Biggs, W. H., III, Kitamura, T., Cavenee, W. K., Wright, C. V., Arden, K. C., and Accili, D. (2002) *Nat. Genet.* **32,** 245–253
42. Kamei, Y., Mizukami, J., Miura, S., Suzuki, M., Takahashi, N., Kawada, T., Taniguchi, T., and Ezaki, O. (2003) *FEBS Lett.* **536,** 232–236
43. Puigserver, P., Rhee, J., Donovan, J., Walkey, C. J., Yoon, J. C., Oriente, F., Kitamura, Y., Altomonte, J., Dong, H., Accili, D., and Spiegelman, B. M. (2003) *Nature* **423,** 550–555
44. Ogg, S., Paradis, S., Gottlieb, S., Patterson, G. I., Lee, L., Tissenbaum, H. A., and Ruvkun, G. (1997) *Nature* **389,** 994–999
45. Brennan, K. J., and Hardeman, E. C. (1993) *J. Biol. Chem.* **268,** 719–725
46. Nagy, T. R., and Clair, A. L. (2000) *Obes. Res.* **8,** 392–398
47. Hahn, C. G., and Covault, J. (1990) *Anal. Biochem.* **190,** 193–197
48. Ogilvie, R. W., and Feeback, D. L. (1990) *Stain Technol.* **65,** 231–241
49. Takahashi, M., Tsuboyama-Kasaoka, N., Nakatani, T., Ishii, M., Tsutsumi, S., Aburatani, H., and Ezaki, O. (2002) *Am. J. Physiol.* **282,** G338–G348
50. Adams, M. D., Kerlavage, A. R., Fleischmann, R. D., Fuldner, R. A., Bult, C. J., Lee, N. H., Kirkness, E. F., Weinstock, K. G., Gocayne, J. D., White, O., *et al.* (1995) *Nature* **377,** 3–174
51. Furukawa-Hibi, Y., Yoshida-Araki, K., Ohta, T., Ikeda, K., and Motoyama, N. (2002) *J. Biol. Chem.* **277,** 26729–26732
52. Tran, H., Brunet, A., Grenier, J. M., Datta, S. R., Fornace, A. J., Jr., DiStefano, P. S., Chiang, L. W., and Greenberg, M. E. (2002) *Science* **296,** 530–534
53. Furuyama, T., Kitayama, K., Yamashita, H., and Mori, N. (2003) *Biochem. J.* **375,** 365–371
54. Garry, D. J., Ordway, G. A., Lorenz, J. N., Radford, N. B., Chin, E. R., Grange, R. W., Bassel-Duby, R., and Williams, R. S. (1998) *Nature* **395,** 905–908
55. Lecker, S., Jagoe, R., Gilbert, A., Gomes, M., Baracos, V., Bailey, J., Price, S., Mitch, W., and Goldberg, A. (2004) *FASEB J.* **18,** 39–51
56. Ezaki, O. (1997) *Biochem. Biophys. Res. Commun.* **241,** 1–6
57. Chakravarthy, M., Davis, B., and Booth, F. (2000) *J. Appl. Physiol.* **89,** 1365–1379
58. Machida, S., Spangenburg, E., and Booth, F. (2003) *J. Cell. Physiol.* **196,** 523–531
59. Yamanouchi, K., Soeta, C., Suzuki, S., Hasegawa, T., Naito, K., and Tojo, H. (2000) *J. Vet. Med. Sci.* **62,** 1213–1216
60. Sandri, M., Sandri, C., Gilbert, A., Skurk, C., Calabria, E., Picard, A., Walsh, K., Schiaffino, S., Lecker, S., and Goldberg, A. (2004) *Cell* **117,** 399–412
61. Stitt, T., Drujan, D., Clarke, B., Panaro, F., Timofeyva, Y., Kline, W., Gonzalez, M., Yancopoulos, G., and Glass, D. (2004) *Mol. Cell* **14,** 395–403
62. Schneider, M., Wolf, E., Hoeflich, A., and Lahm, H. (2002) *J. Endocrinol.* **172,** 423–440
63. Kamei, Y., Ohizumi, H., Fujitani, Y., Nemoto, T., Tanaka, T., Takahashi, N., Kawada, T., Miyoshi, M., Ezaki, O., and Kakizuka, A. (2003) *Proc. Natl. Acad. Sci. U. S. A.* **100,** 12378–12383

Toolbox

Physiol Genomics 21: 274–283, 2005.
First published February 15, 2005; doi:10.1152/physiolgenomics.00107.2004.

A meta-clustering analysis indicates distinct pattern alteration between two series of gene expression profiles for induced ischemic tolerance in rats

Makoto Kano,[1] Shuichi Tsutsumi,[2] Nobutaka Kawahara,[3,4] Yan Wang,[3] Akitake Mukasa,[2,3] Takaaki Kirino,[3,4] and Hiroyuki Aburatani[2]

[1]*Intelligent Cooperative System, Department of Information Systems, Research Center for Advanced Science and Technology, University of Tokyo, Tokyo;* [2]*Genome Science Division, Research Center for Advanced Science and Technology and* [3]*Department of Neurosurgery, Faculty of Medicine, University of Tokyo, Tokyo; and* [4]*Solution-Oriented Research for Science and Technology/Japan Science and Technology, Kawaguchi, Saitama, Japan*

Submitted 5 May 2004; accepted in final form 11 February 2005

Kano, Makoto, Shuichi Tsutsumi, Nobutaka Kawahara, Yan Wang, Akitake Mukasa, Takaaki Kirino, and Hiroyuki Aburatani. A meta-clustering analysis indicates distinct pattern alteration between two series of gene expression profiles for induced ischemic tolerance in rats. *Physiol Genomics* 21: 274–283, 2005. First published February 15, 2005; doi:10.1152/physiolgenomics.00107.2004.—We have developed a visualization methodology, called a "cluster overlap distribution map" (CODM), for comparing the clustering results of time series gene expression profiles generated under two different conditions. Although various clustering algorithms for gene expression data have been proposed, there are few effective methods to compare clustering results for different conditions. With CODM, the utilization of three-dimensional space and color allows intuitive visualization of changes in cluster set composition, changes in the expression patterns of genes between the two conditions, and relationship with other known gene information, such as transcription factors. We applied CODM to time series gene expression profiles obtained from rat four-vessel occlusion models combined with systemic hypotension and time-matched sham control animals (with sham operation), identifying distinct pattern alteration between the two. Comparisons of dynamic changes of time series gene expression levels under different conditions are important in various fields of gene expression profiling analysis, including toxicogenomics and pharmacogenomics. CODM will be valuable for various types of analyses within these fields, because it integrates and simultaneously visualizes various types of information across clustering results.

time series; transcription factor; visualization

ADVANCES IN MICROARRAY TECHNOLOGIES have made it possible to comprehensively measure gene expression profiles. Observation of dynamic changes of gene expression levels provides important markers to clarify cellular responses, differentiation, and genetic regulatory networks. In particular, a comparison of dynamic changes of time series gene expression levels under various conditions (e.g., administration of different drugs) is expected to make a major contribution to the understanding of complex biological processes. In general, we observe the influence of each condition through the results of clustering analysis, which is the most popular analysis for gene expression profiles. Therefore, a comparison between the results of clustering analyses in different conditions will allow interpretation of different macroscopic phenomenon that occurred under those conditions. However, although many clustering algorithms, including hierarchical clustering (1, 2, 4, 15), k-nearest neighbor (17), and self-organizing maps (10, 13, 16) have been proposed, there are few effective methods to effectively compare clustering results under different conditions. We have defined four issues to be addressed for a comparison of clustering results, especially for a comparison of time series gene expression data under two different conditions: changes in the composition of the cluster sets, changes in the expression patterns, integration with known other gene information, and threshold problems.

Changes in the Composition of the Cluster Sets

In this report, we focused on hierarchical clustering, since it is the most popular method for gene expression analysis. Here we define the composition of a cluster set as the hierarchical structure of clustering results and "cluster set" as the set of all clusters in the structure. A comparison of clusters' compositions shows which clusters are conserved in different conditions and how the genes in a cluster for one condition are distributed into a cluster set under another condition. Genes that cluster under a single condition may possibly be regulated by the same factors for that condition. However, under different conditions, some of those genes would be regulated by other factors and generate different clusters. Thus changes in the cluster compositions could provide key information for interpreting the effects of the different conditions. To get a full picture of the relationships of two cluster sets, the overlap between each pair of clusters under the two different conditions should be evaluated. However, since clustering analysis, especially hierarchical clustering, almost always generates a great number of clusters, there are a very large number of combinations of clusters. Simple line connections of the genes between the dendrograms of two hierarchical clustering results (14) provide insufficient information about the relationships between the clusters. Therefore, an effective presentation method that provides a full picture of the relationships of the cluster sets would be desirable.

Recently, a statistical model for performing meta-analysis of independent microarray data sets was proposed (12). This model revealed, for example, that four prostate cancer gene expression data sets shared significantly similar results, independent of the method and technology used. However, in a comparison of the cluster sets based on different conditions, the objective is not to confirm that several data sets share significantly similar results, but to detect the differences be-

Article published online before print. See web site for date of publication (http://physiolgenomics.physiology.org).

Address for reprint requests and other correspondence: M. Kano, Intelligent Cooperative System, Dept. of Information Systems, Research Center for Advanced Science and Technology, Univ. of Tokyo, Tokyo 153-8904, Japan (E-mail: mkano@cyber.rcast.u-tokyo.ac.jp).

tween them. Several statistical algorithms have been proposed for evaluating how clusters based on expression profiles include genes with well-known functions (3, 17). However, the number of clusters that were compared was limited, and an effective presentation method was not required in those situations.

Changes in the Expression Pattern

Where two clusters under different conditions have a statistically meaningful number of genes in common, it is also important to examine the differences in their expression patterns. The differences of macroscopic phenomena that the conditions exhibit result from the differences of expression of multiple, rather than single, genes. Therefore, the genes whose expression patterns changed in a similar fashion between different conditions provide markers for the different phenomena. In other words, if the genes in a certain cluster based on one condition also constitute a cluster for another condition, but the expression patterns are greatly different between the two conditions, then these genes are causally implicated in the phenotypic difference.

In general, there will be many false candidate genes whose expression patterns coincidentally match between the two different conditions. Therefore, it is important to simultaneously evaluate the statistical significance of the overlaps between clusters and the differences in their expression patterns.

Integration with Other Known Gene Information

In gene expression analysis, it is important to biologically interpret the results after integrating them with other known gene information. Therefore, changes in the composition of the cluster sets and changes in the expression patterns between different conditions should be associated with other known gene information such as transcription factors.

Threshold Problems

In a comparison of cluster sets on gene expression profiles, we have to handle four types of thresholds: *1*) a threshold for generating clusters for each condition; *2*) a threshold for evaluating the number of common genes that two clusters have; *3*) a threshold for evaluating the differences in the expression patterns between two clusters; and *4*) a threshold for evaluating the relationship with other known gene information. Among these, determining the threshold for generating clusters is most challenging, because the clustering result strongly depends on this threshold, and a change of this threshold greatly affects the number and composition of clusters. It is generally difficult to determine optimal values for these four types of thresholds, and the results of analysis are greatly affected by the threshold values specified. Arbitrary selection of thresholds involves a risk of overlooking important genes, so the number of thresholds should be reduced, and, if used, it is necessary to allow users to interactively change the thresholds.

We focused on visualization technology to address these four issues. Interactive visualization is effective for handling ambiguous threshold problems and for providing a wide variety of information at one time. In previous work, we developed a "cluster overlap distribution map" (CODM), which is a visualization method for comparing cluster sets based on different sets of gene expression profiles (7). In this report, we extended it for time series gene expression analysis. In the CODM, the relationships of all possible pairing of clusters can be examined, and both the changes in the composition of the cluster sets and the changes in the expression patterns of the clusters can be effectively visualized as three-dimensional (3D) histograms, without any arbitrary thresholds. In addition, relationships with other known gene information such as transcription factors can also be elucidated. We applied the CODM to a comparison between the gene expression data sets of double ischemia rats and sham control rats (with sham operation) and confirmed that CODM identified distinct patterns between the two.

CODM, available on our web site (**http://www.genome.rcast.u-tokyo.ac.jp/CODM**), runs on a PC with Windows 2000 or Windows XP. Memory requirement is in proportion to the square of the number of genes to be analyzed. The analysis for ~4,000 genes, represented in this paper, required ~250 megabytes. In addition, since the analysis results of the CODM are visualized by use of the OpenGL, a machine with a graphics board with a hardware accelerator for the OpenGL is recommended.

MATERIALS AND METHODS

Experiment Design

In this report, CODM is illustrated using time series gene expression data sets obtained from rat four-vessel occlusion models combined with systemic hypotension and time-matched control animals with sham operation. In the experiment, we used 2-min ischemia rats with induced ischemic tolerance (tolerant rats, TOL) and rats with sham operation (sham rats, SHAM), after confirming the histological outcomes. Note that the sham rats did not acquire ischemic tolerance. Three days after the operation, we conducted a 6-min ischemia operation on the two groups. Because of their ischemic tolerance, very little neuronal death of CA1 hippocampal neurons was observed in the tolerant rats (9). With duplicate assessments of 6 time points ({0 h, 1 h, 3 h, 12 h, 24 h, 48 h} × 2) after the second ischemia, microdissected CA1 regions from each of the two groups were subjected to oligonucleotide-based microarray analysis.

All animal-related procedures were conducted in accordance with guidelines for the care and use of laboratory animals set out by the National Institutes of Health and were approved by the committee for the use of laboratory animals in the University of Tokyo. More detailed experimental design is described in our previous report (8).

GeneChip Experiment

Five micrograms of total RNA from each sample was used to synthesize biotin-labeled cRNA, which was then hybridized to a high-density oligonucleotide array (GeneChip Rat RG-U34A array, Affymetrix) essentially following a previously published protocol (6). The arrays contain probe sets for 8,737 rat genes and expressed sequence tags (ESTs), which were selected from Build 34 of the UniGene Database (derived from GenBank 107, dbEST/11-18-98). Sequences and GenBank accession numbers of all probe sets are available from the Affymetrix home page (**http://www.affymetrix.com/index.affx**). Washing and staining was performed in a Fluidics Station 400 (Affymetrix) using the protocol EukGE-WS2. Scanning was performed on an Affymetrix GeneChip scanner to collect primary data. The Affymetrix Microarray Suite v4.0 was used to calculate the average difference for each gene probe on the array, which was shown as an intensity value of gene expression defined by Affymetrix using their algorithm. The average difference has been shown to quantitatively reflect the abundance of a particular mRNA molecule in a

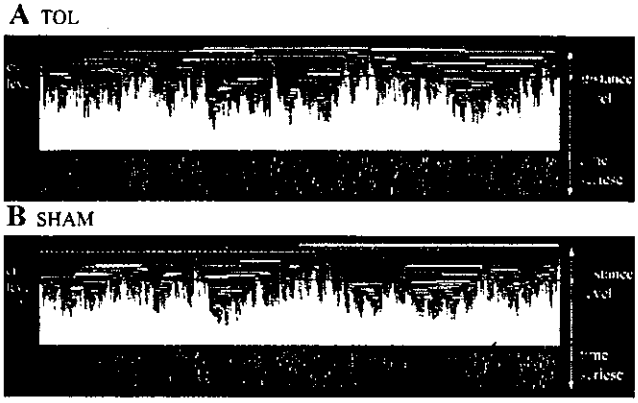

Fig. 1. Hierarchical clustering of TOL (*A*) and SHAM (*B*). We obtained time series ({0 h, 1 h, 3 h, 12 h, 24 h, 48 h} × 2) microarray data from rats with induced ischemic tolerance (tolerant rats, TOL) and rats with sham operation (sham rats, SHAM). In the analysis, we used these data sets as 12 time point ({0a, 0b, 1a, 1b, 3a, 3b, ..., 48a, 48b} = {T_i} (i = 1,2,. . .,12)) data sets on TOL and SHAM, respectively. After preprocessing and normalization, hierarchical clustering analysis based on Euclidian distances was then performed for each data set independently.

population (6). To allow comparison among multiple arrays, the average differences were normalized for each array by assigning the mean of overall average difference values to be 100. This data set has been submitted as GSE1357 to the National Center for Biotechnology Information (NCBI) Gene Expression Omnibus (**http://www.ncbi.nlm.nih.gov/geo/info/linking.html**)

Preprocessing and Clustering

In the following analysis, we used data sets as 12 time point ({0a, 0b, 1a, 1b, 3a, 3b, ..., 48a, 48b} = {T_i} (i = 1,2,. . .,12)) data sets on TOL and SHAM, since the CODM does not depend on the intervals of the time points.

Standard clustering analysis for gene expression profiles is based on the correlation coefficients between genes. Therefore, this approach cannot handle genes with expression profiles that have almost no changes for a condition. However, if the expression profiles of those genes have meaningful changes in expression levels for other conditions, then these provide markers to interpret the influence that the conditions exerted, because these are possibly regulated by different factors. To handle those genes and to align the baselines of the expression patterns between the different data sets, preprocessing (i.e., filtering and normalization) was conducted for all of the data sets where TOL and SHAM were merged. More specifically, 3,363 probes with mean expressions above 50 and coefficient of variance (CV = standard deviation/mean) above 0.1 were selected. After logarithmic transformation of the gene expression data, the expression levels were normalized to satisfy the following equations:

$$\sum_{i}^{12}(x_i + y_i) = 0 \qquad (1)$$

$$\sum_{i}^{12}(x_i^2 + y_i^2) = 1 \qquad (2)$$

where x_i and y_i are normalized expression levels of a gene at time point T_i (i = 1,2,. . .12) on conditions TOL and SHAM, respectively. Using these normalized data sets, we performed hierarchical clustering analysis based on Euclidian distances, for each data set independently. Clustering analysis using Euclidian distances instead of correlation coefficients allows us to handle genes whose expression levels are downregulated or upregulated. In addition, due to the common normalization, gene expression patterns can be compared within a data set and between data sets.

In general, Euclidian-distance-based clustering after normalization, in terms of mean and standard deviation, is equivalent with correlation-coefficient-based clustering. That is, a Euclidian-distance-based clustering analysis for the merged data of TOL and SHAM with the above preprocessing is equivalent with a correlation-coefficient-based clustering analysis for the original merged data. In the analysis of the CODM, the preprocessing is conducted for the merged data, and Euclidian-based clustering is individually conducted for each data. Roughly speaking, this analysis provides us with results similar to those of normal correlation-coefficient-based clustering, while it allows us to handle genes with expression profiles that have changes for only one condition but not for the other.

As Fig. 1, *A* and *B*, shows, there are a large number of clusters generated at various levels. Although the composition and number of cluster sets depend on the threshold value of the distance, it is generally difficult to identify an optimum value. These aspects make it difficult to compare cluster sets derived from different sources.

The Cluster Overlap Distribution Map

The CODM is a visualization methodology for pair-wise comparison between cluster sets generated from different gene expression data sets. In this methodology, two types of cluster sets (i.e., dendrograms of hierarchical clustering results) are mapped, respectively, to the x-axis and to the y-axis, and the relationship between them is displayed as a 3D histogram (Fig. 2). In this report, the dendrogram of TOL is mapped to the x-axis, and that of SHAM is mapped to the y-axis. The statistical evaluation values of the overlaps between two clusters selected from the respective cluster sets are displayed as the height of the blocks (Fig. 2). More specifically, we evaluated the number of common genes between the two different clusters by using hypergeometric probability distributions (17). Assuming that the generation of gene clusters is a random selection from among the total set of genes, the probability of observing at least k overlapping genes between randomly selected n_1 genes and n_2 genes from among all of the g genes is given by:

$$P(g,n_1,n_2,k) = 1 - \sum_{i=k}^{k-1} \frac{{}_{n_2}C_i \cdot {}_{g-n_2}C_{n_1-i}}{{}_{g}C_{n_1}} [= P(g,n_2,n_1,k)] \qquad (3)$$

When the P value is small, the overlap is regarded as statistically meaningful. Thus we defined the evaluation value of the overlap as:

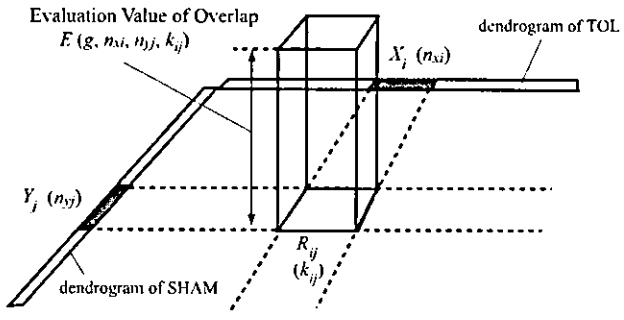

Fig. 2. Overlap block of two clusters. The dendrogram of TOL is mapped to the x-axis, and that of SHAM is mapped to the y-axis. Then, for the area (R_{ij}) determined by a cluster on the x-axis (X_i) and a cluster on the y-axis (Y_j), a block whose height represents $E(g,n_{xi},n_{yj},k_{ij})$ (statistical evaluation values of the overlaps between X_i and Y_j) is displayed, where g is the total number of genes, n_{xi} is the number of genes in X_i, n_{yj} is the number of genes in Y_j, and k_{ij} is the number of overlap genes between X_i and Y_j.

$$E(g,n_1,n_2,k) = -\log_{10}P(g,n_1,n_2,k) \quad (4)$$

Then in the area (R_{ij}) determined by a cluster on the x-axis (X_i) and a cluster on the y-axis (Y_j), a block whose height represents $E(g,n_{xi},n_{yj},k_{ij})$ is displayed, where n_{xi} is the number of genes in X_i, n_{yj} is the number of genes in Y_j, and k_{ij} is the number of overlapping genes between X_i and Y_j (Fig. 2). We term this block an "overlap block." Note that the number of UniGenes, to which probes in a cluster correspond through their original GenBank accession number, was used as the number of genes. In this report, all 8,737 probes on RG-U34A were corresponding to 5,249 UniGenes (g = 5,249).

For hierarchical clustering, there are a large number of clusters generated at various distance levels. Our algorithm examines the overlaps of the genes between all combinations of two clusters with smaller "distance level" values than the "cut level," which is a threshold value specified by users (Fig. 1). In other words, we evaluated and visualized any clusters with a smaller distance level than the cut level, even if they were included in other clusters. Note that conventional hierarchical clustering does not focus on subclusters that are included in other clusters. Since all of the statistically significant combinations between cluster sets can be visualized simultaneously, users can grasp the overall picture of the relationships between the two different cluster sets.

In the CODM, all of the clusters are dealt with equally without regard to their difference level (i.e., their homogeneity). Even if they are included in other clusters, all of the statistical significance of the number of common genes between clusters is simultaneously visualized. Therefore, there is a risk that a small overlap block may be hidden by a large block. For example, assume that the clusters X_j and Y_n are included in X_i and Y_m respectively. Then, if the evaluation value E_{jn} is less than E_{im}, then the small block B_{jn} will be hidden in the large block B_{im} (Fig. 3*A*). To avoid this problem, the CODM allows the user to change the cut level interactively. That is, if the user decreases the cut level, some small blocks that are hidden in larger blocks will emerge. Therefore, in consideration of the homogeneity of clusters and the relationships with other gene information, the user can find important genes displayed as blocks in the CODM.

Color of Each Overlap Block

Since the statistical significance of the number of common genes between two different clusters is represented as the height of a block, the color of a block can be used to represent other information. In the current prototype, the CODM provides three color modes.

1) Redundant visualization. The first mode is a representation of the evaluation values of overlaps using a gray scale. This redundant representation helps users comprehend the distribution of the relative evaluation values of overlaps.

2) Similarity of expression patterns. The second mode is a representation of the similarity of expression patterns between two clusters, from red to blue. The similarity $f(T,S)$ of expression patterns between *cluster T* on TOL and *cluster S* on SHAM was defined using the average of the square of the Euclidean distance between them. Assuming that N_{TS} is the number of common genes in T and S, x_{ki} and y_{ki} are normalized expression levels of a common gene k at time T_i on TOL and SHAM, respectively. The similarity $f(T,S)$ was defined as follows:

$$f(T,S) = 1 - \frac{1}{N_{TS}} \sum_{k=1}^{N_{TS}} \sum_{i=1}^{12} (x_{ki} - y_{ki})^2 \quad (5)$$

Since $\{x_{ki}\}$ and $\{y_{si}\}$ (i = 1,2,. . .12) satisfy *Eqs. 1* and *2*, the range of $f(T,S)$ is -1 to 1, and $f(T,S)$ can be rewritten as follows (See APPENDIX):

$$f(T,S) = \frac{1}{N_{TS}} \sum_{k=1}^{N_{TS}} \sum_{i=1}^{12} 2x_{ki}y_{ki} \quad (6)$$

In the CODM, the similarity $f(T,S)$ was represented as the color of the block from red ($f(T,S)$ = 1) to blue ($f(T,S)$ = -1). Roughly speaking, red indicates that expression patterns between the two clusters are similar, and blue indicates they have a negative correlation. In addition, purple ($f(T,S)$ = 0) indicates they have no correlation, or genes of one cluster have no changes in expression levels, i.e.,

$$\forall x_{ki} \approx 0 \text{ or } \forall y_{ki} \approx 0$$

As mentioned above, if genes in a certain cluster based on SHAM also constitute a cluster in TOL, but the expression level in SHAM is significantly different from that in TOL, then these genes provide potential markers for the cause of ischemic tolerance. Strong candidates will appear as tall blue or purple blocks. CODM allows users to easily look for such blocks, with interactively controlling the thresholds.

3) Relationship with a known gene classification. The third type of information is a representation of the relationship between overlapping genes and a known gene classification. If statistically significant representation of genes within a particular class is observed among the overlapping genes, then the block is color coded according to the class. The level of statistical significance of the representation of genes within a particular class is evaluated using *Eq. 3*, where g is the total number of genes that are classified by the known classification, n_1 is the number of genes that are classified by the known classification among overlapping genes, n_2 is the total number of genes within a class based on the known gene classification, and k is the observed number of genes found in both the given overlapping genes and the given class according to the known gene classification.

In this report, we associated overlapping genes with eight types of transcription factors (HIF, ARNT, and EGR families) that were reported to have a relationship with ischemia (5, 8, 18, 19). We extracted complete sequences of 1.0 kb upstream and 0.1 kb downstream for 2,816 UniGenes among the 5,249 UniGenes corresponding to 8,737 probes on the RG-U34A microarray. The 1.1-kb sequences of the 2,816 UniGenes were searched to determine whether they correspond to the TRANSFAC matrices v7.2 (11) with the threshold set to "minimum false negative." Table 1 shows the names of the transcription factors, the number of UniGenes that correspond to each transcription factor, and the thresholds for matching. In CODM, we color

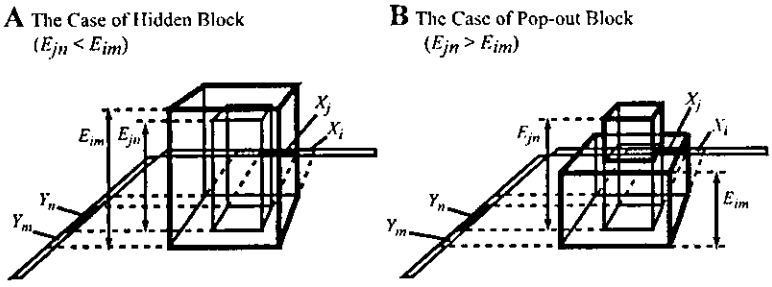

Fig. 3. Relationships of two blocks. In CODM, all of the clusters are dealt with equally, regardless of their difference levels (i.e., their homogeneity). Even if they are included in other clusters, all of the statistical significance of the number of common genes between clusters is simultaneously visualized. There is a risk that a small overlap block may be hidden in a large block. Assume that the clusters X_j and Y_n are included in X_i and Y_m, respectively. Then, if the evaluation value E_{jn} is less than E_{im}, the small block B_{jn} will be hidden within the large block B_{im} (*A*).

Table 1. *Transcription factors linked to ischemia*

Transcription Factor	No. of UniGenes	Thresholds
V$AHRARNT_01	540	0.92
V$AHRARNT_02	4	0.91
V$HIF1_Q3	955	0.55
V$HIF1_Q5	507	0.87
V$EGR1_01	143	0.87
V$EGR2_01	92	0.89
V$EGR3_01	26	0.93
V$ENGFIC_01	143	0.88

In the cluster overlap distribution map (CODM), changes in the composition of the cluster sets and changes in the expression patterns between different conditions were associated with 8 types of transcription factors (HIF, ARNT, and EGR families), which are all known to mediate response to ischemia. We extracted UniGenes that contain putative binding sites for the transcription factors and correspond to probes on RG-U34A GeneChips (Affymetrix, Santa Clara, CA). Shown are the names of the transcription factors, the number of UniGenes, and the thresholds for matching.

coded overlap blocks that contain statistically meaningful numbers of genes with putative transcription factor binding sites. If an overlap block represents statistical significance for multiple transcription factors' putative binding sites, then only a single transcription factor with the highest evaluation value was visualized. However, the CODM allows users to click overlap blocks and browse description messages (in a console window) for the relationships with all of the transcription factors.

RESULTS AND DISCUSSION

Figure 4 shows the visualization results of the comparison between TOL and SHAM in the mode of redundant visualization, the similarity of the expression patterns, and the relationships with known gene classifications (transcription factors). In Fig. 4, the cut level for the distance for hierarchical clustering was 0.74, and all overlap blocks with 2.0 or higher evaluation values are displayed as a 3D histogram. As Fig. 4 shows, the CODM provides not only a 3D mode but also a two-dimensional (2D) mode where users can see a projected overhead view of the 3D mode. In the 3D mode, the statistical significance of the overlaps between clusters and the differences in expression levels between the clusters can be simultaneously represented, since we can use the height and color of blocks. However, it is somewhat difficult to recognize the expression patterns of clusters that generate an overlapping block. For this purpose, the 2D mode is better, although the 2D mode of CODM can visualize only a single species of information at a time, i.e., the statistical significance of the overlaps or the differences in expression levels between clusters, or relationships with known gene classification. Therefore, it is useful to interactively change the mode as required. Exploration by changing the color mode and the 2D and 3D modes allowed us to pick up three potentially important overlap blocks (Fig. 4). The information for these three overlap blocks is shown in Table 2, their gene lists are shown in the Supplemental Material, and their expression patterns are shown in Fig. 5. (The Supplemental Material is available at the *Physiological Genomics* web site.)[1]

[1]The Supplemental Material (Supplemental Tables S1–S3) for this article is available online at **http://physiolgenomics.physiology.org/cgi/content/full/00107.2004/DC1**.

As stated above, we assumed that there are four issues for a comparison of clustering results: changes in the composition of the cluster sets, changes in the expression patterns, relationships with other known gene information, and threshold problems. The CODM enables us to address these issues as follows.

Changes in the Composition of the Cluster Sets

As shown in Fig. 4, *A* and *B*, the CODM can intuitively visualize changes in the composition of the cluster sets as 3D histograms. That is, the dissimilarity of the expression level under SHAM divides each cluster on TOL into specific subclusters, and these subclusters are displayed along the *y*-axis. In the same manner, the relationships between each cluster of SHAM and all of the clusters of TOL are displayed on the *x*-axis. If a clustering analysis is conducted for the merged data of TOL and SHAM, then these subclusters would be scattered and it would be difficult to intuitively observe the relationships of the compositions of the cluster sets.

Changes in the Expression Pattern

A comparison of the dynamic changes of gene expression level across time under various conditions provides a useful tool for interpreting complex biological processes. However, there are generally many false candidate genes whose expression patterns between two different conditions are different purely by chance. For the comparison between TOL and SHAM, only 357 probes (of the 3,363 selected probes) had 0.8 or higher correlation coefficient values of expression pattern between the two conditions. On the other hand, 756 probes had negative correlation coefficient values. As stated above, the difference of macroscopic phenomena that the conditions exhibit results from the difference of expression of not a single gene but of multiple genes. Therefore, it is quite important to search for genes whose expression patterns changed in a similar fashion between different conditions. Figure 4, *C* and *D*, shows that the CODM can simultaneously depict the statistical significance of the overlaps between clusters and the differences in their expression patterns. In this mode, tall blocks colored blue or purple, such as *blocks B* and *C*, would be good candidates, since their similarities of expression patterns were negative (-0.28 and -0.23), while the two clusters under different conditions share a statistically meaningful number of common genes ($E = 53.3$ and $E = 34.8$). Note that the objective of the CODM is to identify such potentially important pairs of clusters from massive combinations. To further understand the significance of the expression patterns, it would be a desirable approach to combine CODM with other visualization tools for line graphical view of expression patterns, as shown in Fig. 5. The expression of genes in TOL in *block B* was upregulated, compared with SHAM, at early stage, i.e., 1 h, 3 h, and 12 h. On the other hand, the expression of genes in TOL in *block C* was downregulated, compared with SHAM, at early stage, i.e., 1 h, and 3 h. Once again, CODM enabled us to easily detect candidate genes of this type.

Integration with Other Known Gene Information

In gene expression analysis, interpretation and validation of the results should be performed in the context of what is already known about the genes being analyzed. CODM allows us to associate the results with other such gene information and

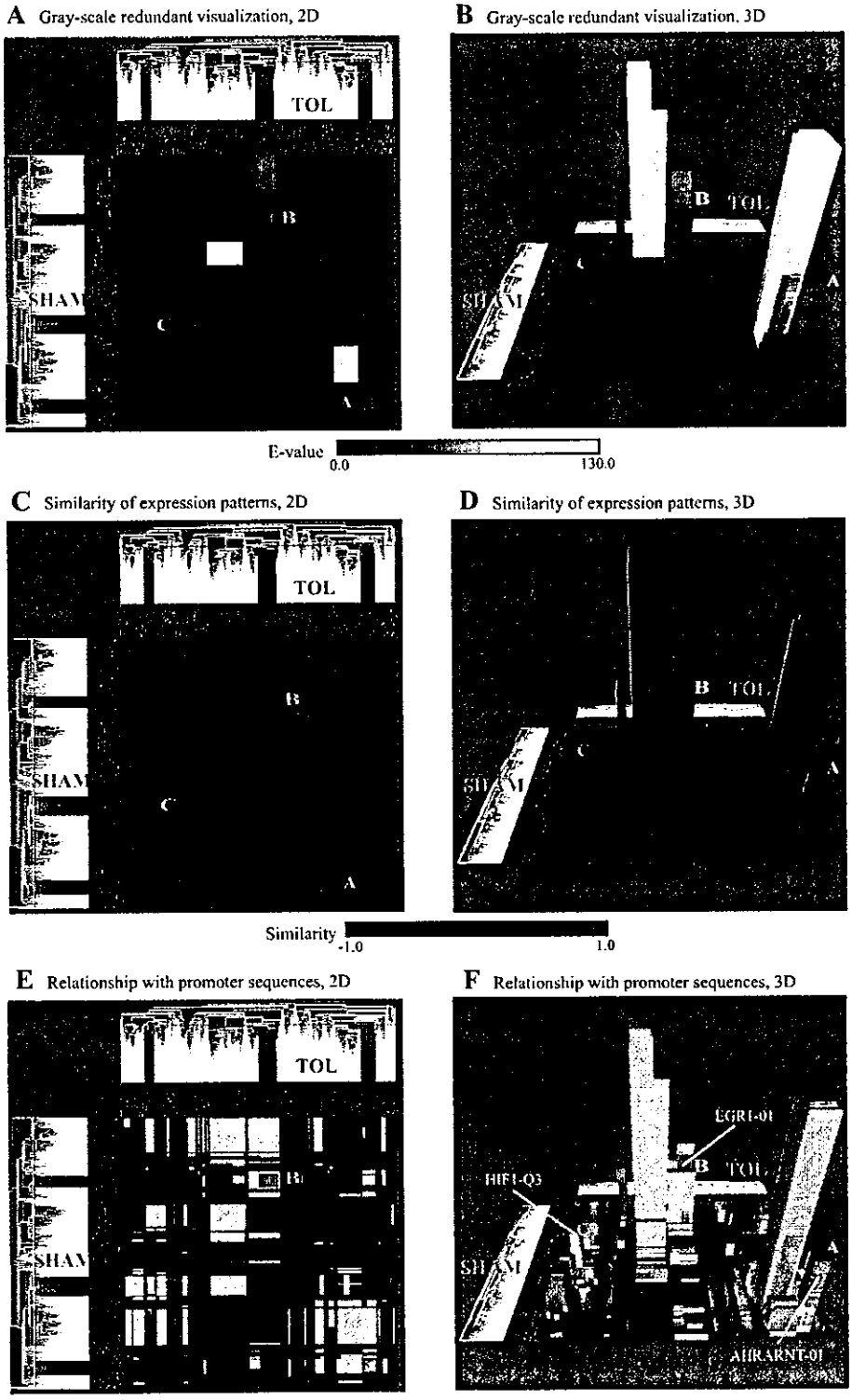

Fig. 4. Visualizations for comparison of clustering results of TOL and SHAM. These are visualization results of the comparisons between TOL and SHAM in the mode of redundant visualization (*A* and *B*), similarity of the expression patterns (*C* and *D*), and the relationships with transcription factors (*E* and *F*). Here, the cut level of the distance for hierarchical clustering was 0.74, and all of the overlap blocks with 2.0 or higher evaluation values are displayed as three-dimensional (3D) histograms. As shown, the CODM provides not only a 3D mode (*B*, *D*, and *F*) but also a two-dimensional (2D) mode (*A*, *C*, and *E*) where users can see a projected overhead view of the 3D mode. In the mode showing the relationships with the transcription factors (*E* and *F*), we considered the relationships with 8 types of transcription factors (HIF, ARNT, and EGR families) that are known to mediate response to ischemia. Here, only overlap blocks with 2.0 or higher evaluation values of the number of genes with putative transcription factor binding sites were color coded. Where an overlap block represents statistical significance for multiple transcription factors' putative binding sites, only the transcription factor with the highest evaluation value was visualized. Exploration through changing the color mode and the 2D and 3D mode allowed us to pick up three potentially important overlap blocks that represented high evaluation values of the number of genes with the binding sites ($E > 2.0$).

narrow down candidates. Figure 4, *E* and *F*, shows the relationships between eight types of transcription factors (HIF, ARNT, and EGR families; see Table 1) that were reported to have a relationship with ischemia (5, 8, 18, 19). In Fig. 4, overlap blocks with 2.0 or higher evaluation values for the representation of genes with putative transcription factor binding sites were color coded. Table 2 shows that overlap *blocks A*, *B*, and *C* implied a relationship with the transcription factors ($E > 2.0$). This example illustrates the utility of representing relationships with other known gene-associated information by